DESIGN, SYNTHESIS, AND TRIBOLOGICAL EVALUATION OF POLYMERIC-BASED NANOCOMPOSITES

A Thesis

by

SAYAK CHAKRABORTY

Submitted to the Office of Graduate and Professional Studies of
Texas A&M University
in partial fulfillment of the requirements for the degree of

MASTER OF SCIENCE

Chair of Committee,	Hong Liang
Committee Members,	Dorrin Jarrahbashi
	Alex (Gwo-Ping) Fang
Head of Department,	Andreas A. Polycarpou

December 2019

Major Subject: Mechanical Engineering

ABSTRACT

In the last decade, 3D printing has revolutionized the design and manufacturing industry. Stereolithography (SLA), the most accurate commercially-available form of 3D printing, and the third most commonly used 3D printing method, is used in diverse industries: from automotive to healthcare. One of the main limitations of the SLA process is the limited number of commercially-available high-performance resins. This is the problem that our research has aimed to address. The objective of this research was to design and synthesize a novel polymer-based 3D printable photoactivated nanocomposite that could be used to print parts with superior tribological capabilities.

Layered zirconium hydrogen phosphate with α-type structure, $Zr(HPO_4)_2.H_2O$, a low-cost environmental-friendly anti-wear & anti-friction additive, was chosen as the additive, and standard photoreactive clear resin was chosen as the polymer matrix. Specimens containing a series of concentrations from 0 to 1% (by weight) of α-ZrP nanoparticles were fabricated using two different approaches – casting & 3D printing. The fabricated specimens were subjected to wear & friction tests, using a pin-on-disc tribometer at room temperature. The worn surfaces were characterized using optical microscopy and interferometry.

Samples with 0.1 wt.% of α-ZrP nanoparticles showed promising results. 3D printed samples showed a 65% reduction in wear and a 34% reduction in friction. Similar to 3D printed samples, casted samples exhibited a 67% reduction in wear and a 32% reduction in friction. In comparison between the two fabrication processes, it was observed that 3D printing significantly improves the wear resistance of specimens. 3D printed specimens showed a 40% reduction in wear volume as compared to the casted specimens. This improved performance was attributed to the layer-by-layer printing approach employed in 3D printing, leading to more improved alignment of α-ZrP nanoparticles within each layer of the 3D printed specimens.

The findings of this research are beneficial to the advanced manufacturing and polymer nanocomposite industry, and explore new areas for the application of nanoparticles in synthesizing superior polymer-based 3D-printable nanocomposites.

The thesis consists of six chapters. Chapter I includes background information about stereolithography, tribology and polymer nanocomposites. Chapter II discusses the motivation and objectives. Chapter III discusses experimentation methodologies and materials used in this research. Chapter IV and V present and discuss the results obtained - casted versus 3D printed. Chapter VI provides a summary of the major conclusions obtained from the results, and recommends suggestions for future work.

ACKNOWLEDGEMENTS

I would like to thank my committee chair, Dr. Liang, for mentoring me and guiding me throughout the course of my research. I would like to thank my committee members, Dr. Jarrahbashi and Dr. Fang for their continued guidance and support.

I would also like to thank all the members of the Surface Science Research Group, especially Yan Chen, Eugene Chen and Swarn Jha for all of their help, constructive criticism and guidance.

Thanks also go to my friends and colleagues, and the department faculty and staff for making my time at Texas A&M University a memorable experience.

Finally, all of this would not have been possible without the unwavering support of my family. All of their teachings, guidance, encouragement and sacrifices has led me to where I am today. I am extremely grateful and blessed to have been gifted with such an amazing family.

CONTRIBUTORS AND FUNDING SOURCES

Contributors

This work was supervised by a thesis committee consisting of Dr. Liang and Dr. Jarrahbashi of the Department of Mechanical Engineering and Dr. Fang of the Department of Engineering Technology & Industrial Distribution.

All other work conducted for the thesis (or) dissertation was completed by the student with the help and guidance of the members of the Surface Science group, especially Yan Chen, Eugene Chen and Swarn Jha.

Funding Sources

The research work was supported in part by the Oscar S. Wyatt Jr. Professorship and the Texas A&M Foundation.

NOMENCLATURE

SLA	Stereolithography
NP	Nanoplatelet
3D	Three dimensional
SFF	Solid Free-form Fabrication

TABLE OF CONTENTS

Page

LIST OF FIGURES

Page

LIST OF TABLES

Page

CHAPTER I

INTRODUCTION

This chapter provides background information needed in order for readers to understand the undertaken research. It discusses the origin of additive manufacturing, analyzes in detail the stereolithographic printing process along with the most commonly used photopolymers for stereolithographic printing. This is followed by explaining the concept of tribology, in terms of friction and wear. Subsequently, the characteristics, applications & limitations of traditional micrometer-scale polymer composites are explored, along with considering the pros and cons of using nanoscale-filled polymer composites for overcoming these limitations. Finally, layered zirconium hydrogen phosphate with an α-type structure, $Zr(HPO_4)_2.H_2O$ is considered as a potential nanoparticle additive for designing & synthesizing a novel photoactivated polymer nanocomposite, for use with Stereolithography (SLA), that exhibits superior tribological performance.

1.1. Stereolithography

1.1.1. History of Stereolithography

Within the last decade 3D printing has become an integral part of the design and manufacturing industry. Traditional prototyping methods are time-consuming and require labor-intensive mold-making and casting processes, whereas with 3D printing and solid freeform fabrication, complicated and precise prototypes could be fabricated within a few hours from a CAD file, using rapid prototyping and additive manufacturing techniques, thereby significantly speeding

up product development. Breakthroughs in 3D printing technology have completely transformed the way industries approach prototyping and manufacturing. 3D printing has helped businesses and industries drastically reduce the cost and time associated with prototyping and manufacturing by allowing faster iterations, faster turnaround times, optimizing manufacturing processes and enabling complex product geometries[1].

Since 1981 diverse 3D printing methods have been developed to fabricate complicated 3D structures. Some 3D printing techniques have become more popular than others and have captured a lion's share of the additive manufacturing industry. The most popular 3D technologies widely used in the industry today include[2]:

- Digital Laser Processing
- Digital Beam Melting
- Stereolithography
- Selective Laser Melting
- Selective Laser Sintering
- Laminated Object Manufacturing
- Fused Deposition Modeling

Each method has its own unique setup and can be used to fabricate objects within a specific size range. Each 3D printing technology has a lower limit on the resolution, which indicates the size of the smallest detail that can be fabricated. There exists a simple correlation between the size of a 3D printed object and the resolution with which it is fabricated (applicable for

most SFF techniques); the greater the resolution with which a part can be produced, the lower will be its maximum size and vice versa[3].

Lithography involves fabrication of graphic objects. Modern photolithographic AM systems use photosensitive materials combined with the principle of computer-generated graphics to produce 3D objects. Photolithographic systems fabricate complicated geometries by using light to selectively cure photosensitive resins [4]. There are two fundamental methods:

- Stereolithography
- Photo-mask

Stereolithography is one of the most commonly used 3D printing techniques and it is a part of the vat photopolymerization additive manufacturing technology family. It involves producing solid models by scanning a beam of ultraviolet light over the surface of a photopolymer. Developed in 1986 by 3D Systems, stereolithography was the first commercially available solid freeform fabrication (SFF) technique.

1.1.2. Stereolithographic building process

With respect to other SFF techniques, stereolithography comes out on top in terms of accuracy and resolution. For most fabrication techniques, the object resolution is usually in the range of 50-200 μm, whereas most of the commercially available SLA 3D printers can comfortably

achieve an object resolution of up to 20 μm. Such a high accuracy makes stereolithography the most accurate (commercially available) SFF technique [5].

In any stereolithographic processes, a multi-functional prepolymer is transformed into a cross-linked polymer, through a chain reaction initiated by reactive species generated by light exposure[6]. In any stereolithographic process, initiators (low molecular weight organic molecules) are used to set off the polymerization process. This is because most monomers or prepolymers cannot produce initiating species on their own, upon being exposed to irradiation[6].

In stereolithography, a light source is used to cure light-reactive thermoset materials (liquid resin) into hardened plastic. Photopolymerization process is used in SLA to solidify the liquid resin. In this process, on exposure to specific wavelengths of UV light, the short molecular chains within photopolymer liquid resins join together, polymerizing monomers and oligomers into solidified rigid or flexible geometries[3]. The photopolymerization process is irreversible and once solidified there is no way to convert 3D printed parts back into their previous liquid form.

For stereolithographic resins, the curing process involves an exothermic polymerization process. In this process, chemical cross-linking reactions produce an infusible, insoluble, and highly cross-linked 3D network[4]. Using a specific stereolithographic process, an appropriate

form of energy is provided to initiate the reaction process. Irrespective of the method used to start the polymerization process, two key events occur during the curing process[7]:

- Gelation (involving viscosity increase and transformation of the liquid resin to a rubbery mixture)
- Vitrification (involving transformation of the liquid/rubbery resin to a harder glass-like substance)

A representation of the curing reaction is provided in the Fig. 1.

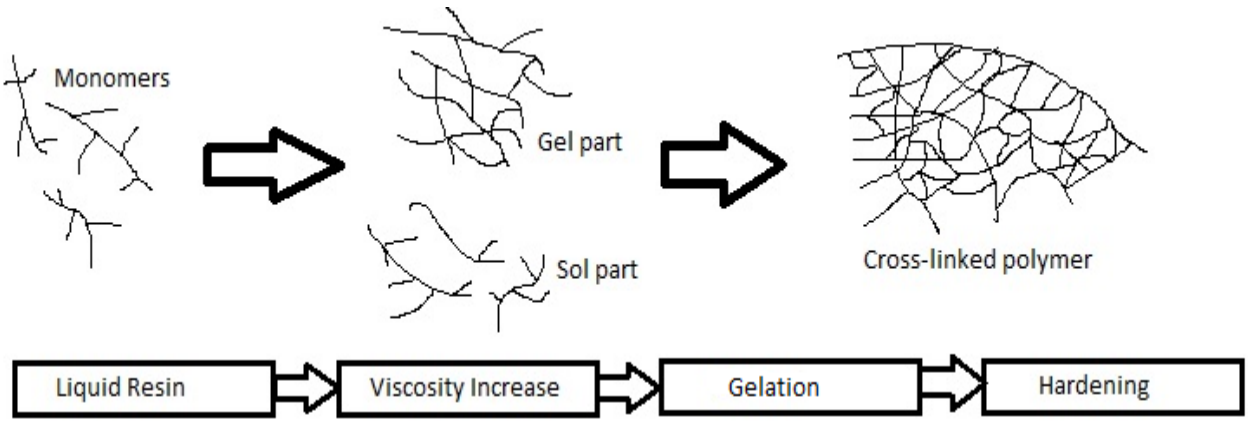

Figure 1. Curing mechanism in stereolithographic processes

The essential steps for manufacturing a 3D printed part using an SLA printer includes [3]:

1. *Part Design*

   The design of the part to be fabricated (including internal and external geometry) can be generated using one of the following methods[8-12]:

a. CAD software – The required file contains information regarding the part geometry and dimension. The CAD file is exported into a 3D printable file format; the STL file format is usually used for this purpose.

b. Mathematical equations – using a microstructural shape design approach, porous 3D printed parts are produced, which utilize spatial periodicity as an efficient and simple to way to generate the part design. A geometric illustration of the topology microstructure is provided using trigonometric and other higher mathematical functions.

c. Scan data of imaging technologies, or tomography techniques - The flexibility of using scan data from imaging technologies such as Magnetic Resonance Imaging (MRI) makes SLA particularly useful for biomedical applications. This particular method of data acquisition allows the fabrication of patient-specific implants[3].

2. *Slicing and 3D printing software*

All SLA printers are provided with software that can be used to specify the printing parameters like layer thickness and model orientation. The software (virtually slices) the 3D model into two-dimensional layers using the layer thickness value provided. Usually the layer thickness values range between 25-100 μm.

3. *Printing*

In stereolithography, the parts are printed using photopolymerization, which involves controlled solidification of a photopolymer resin using an ultraviolet light beam. The actual printing process consists of the following steps:

a. The build platform within the 3D printer is lowered into the liquid resin tank by a distance equal to the print resolution (equal to the thickness of a single layer).
b. A certain wavelength of ultraviolet light is used to cure the resin layer by layer.
c. After a single layer is cured, the platform moves downwards by a distance equal to the print resolution. The UV light scans the next layer on to the resin surface and in this way additional layers are built on top of one another.
d. Once the all the layers have been printed, the vat is drained of resin and the finished part is removed from the build platform.

4. Post-Processing

Once the printing process is completed, the part is taken out of the 3D printer, and rinsed in alcohol (usually isopropyl alcohol). This rinsing process helps to remove any uncured resin from the surface of the 3D printed part. After rinsing the part is left to dry. For some materials, other post-processing processes might be involved. These processes usually help further enhance the strength and stability of the printed parts. Finally, any supports attached to the part are removed/cut off[5].

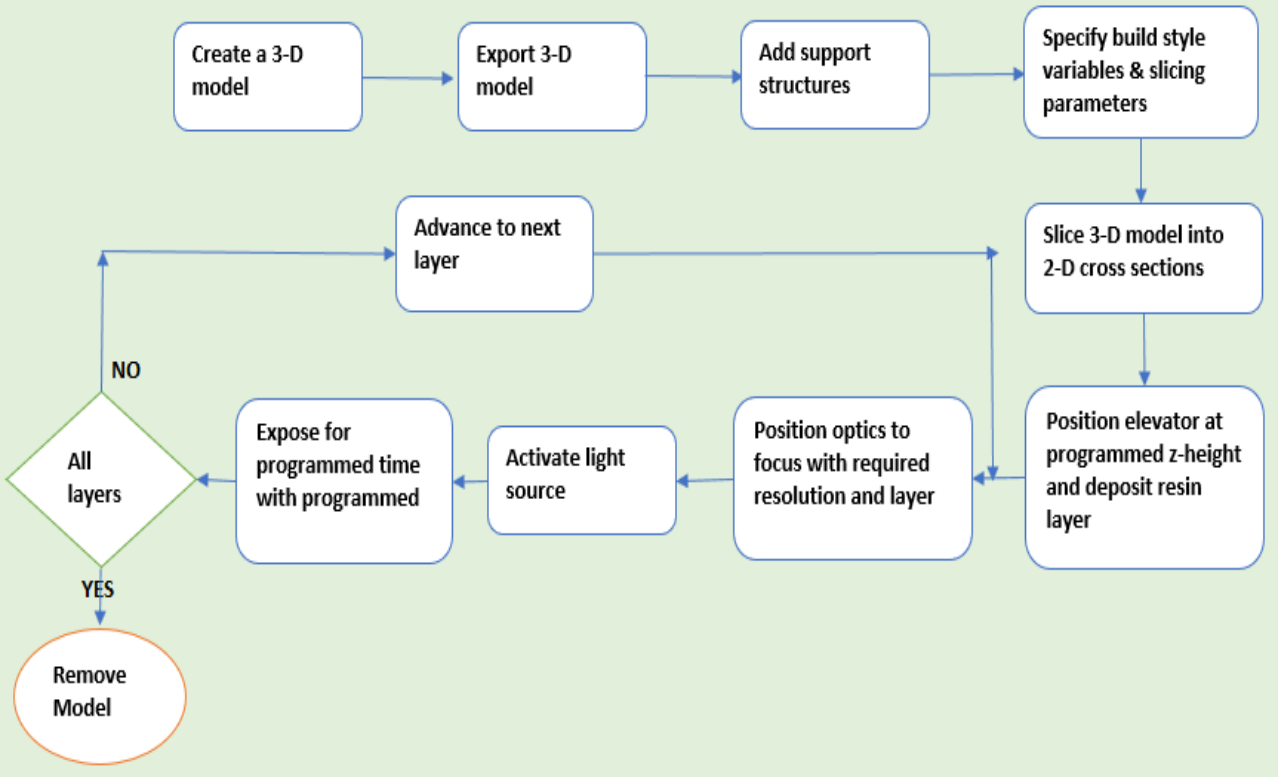

Figure 2. Block diagram of the processes involved in fabrication of structures by stereolithography

1.1.2. Materials for stereolithography

The photopolymer resins commonly used consist of the following components[13]:

- Photoinitiators – The photoinitiator in stereolithography directly controls the rate of the curing process. An acceptablee photoinitiator system provides high initiation efficiency, storage stability, and good solubility in the prepolymer. Usually photoinitiator concentration varies between 0.5% to 12% by weight. They can enable cure depth between 0.1 and 2.5 mm.

- Polymerizable oligomers or prepolymers – Free radical-based systems used to be the most common stereolithographic resins, based on acrylate and methacrylate monomers. The acrylate and methacrylate monomers allow for rapid curing and are easily modifiable at the ester functionality. These characteristics allowed for synthesizing materials with diverse properties.
- Reactive diluent – Low-viscosity monomers are commonly used as reactive diluents. These are mixed with the stereolithographic resins to lower the viscosity of the solution.
- Additives – Additives are materials added (usually in minor quantities) to stereolithographic resin to impart specific enhanced properties to the cured resin. They can be used to affect the final physical/chemical/mechanical/electrical properties of the cured resin, the way the resin is cured, and even the curing time.

The main limitation of the SLA process is considered to be the limited number of commercially-available resins. The main requirement for a resin, to be used for the SLA process, is the ability to solidify rapidly on exposure to a certain-wavelength of light. Low-molecular weight polyacralate or epoxy macromers were the first resins developed for use in stereolithography. They formed glassy networks on photopolymerization[4, 8].

With the breakthroughs in SLA technology, innovative and high-performance SLA resin formulations have been developed by material manufacturers for a wide range of industrial thermoplastic applications, including optical, thermal and mechanical applications. Over the past two decades, several resins have been developed with varying mechanical properties for a wide variety of applications. The physical mechanical, electrical and chemical properties of parts

fabricated using stereolithography are improving continuously and as such the applications for 3D printed parts in functional, demanding end-use applications are growing at a rapid rate.

The main advantages common to SLA materials are [14]:

- Excellent surface finish.
- Refined features and excellent details.
- Increased stiffness.

The limitations common to all SLA materials are:

- Relatively brittle, exhibiting low elongation at failure.
- Overexposure to UV radiation (sunlight) may change material properties over time. As such, for outdoor applications properties of the 3D printed may change over time.
- Susceptible to creep.

The different types of SLA resin commonly used in the industry are listed below[14]:

1. Standard SLA resin
    a. Standard resin - Standard resins are low-cost resins that provide high stiffness and can be used to print parts with high-resolution smooth injection molding-like finishing. They are ideal for concept modeling, and prototyping applications.
    b. Clear resin – They exhibit identical mechanical properties to standard resin. Alongside, with pre-processing, parts printed with clear resin can be developed to

high optical transparency. Prolonged exposure to UV radiation (sunlight) may impact the optical transparency of the printed parts.

2. Engineering resin
    a. Tough resin – This type of resin has been developed for applications requiring high performance in terms of withstanding high values of stress, strain and fatigue. Parts printed using tough resin exhibit high values of tensile strength and modulus of elasticity, comparable to ABS. They are ideal for functional prototyping applications and mechanical assemblies.
    b. Durable resin - This type of resin has exceptional wear resistance and flexibility, with mechanical properties similar to Polypropylene (PP). Parts printed using durable resin exhibit high elongation at break and so are highly flexible. These parts also exhibit low friction and excellent surface finish. They are ideal of functional prototyping applications, low-friction and low-wear mechanical parts, and consumer products.
    c. Heat-resistant resin – This type of resin exhibits a high heat deflection temperature between 200-300°C. Parts printed using heat-resistant resins are best-suited for applications requiring high thermal stability. These resins are best-suited for manufacturing high-temperature fluid flow equipment, heat resistant fixtures, mold prototypes.
    d. Rubber-like resin (Flexible) - These resins have a low tensile modulus and high flexibility (high elongation at break). They can be used to simulate rubber components. Parts printed using rubber-like resins are best suited for applications where the parts would be subjected to bending and/or compression. They are ideal

for prototyping of wearable applications, multi-material assemblies, handles, grips and overmolds,

e. Ceramic-filled resin (Rigid) - Ceramic filled are reinforced with glass or other ceramic particles. Along with offering high heat resistance and thermal stability, they offer high stiffness and very smooth surface finish. They also exhibit lower creep and high modulus of elasticity as compared to other SLA resins.

1.1.3. Comparison of stereolithographic materials

The primary mechanical properties of the SLA resins mentioned above are summarized below [19]:

Table 1. Mechanical properties of common SLA resins. Reprinted from [15]

	Standard & Clear	Tough	Durable	Heat resistant	Ceramic reinforced
IZOD impact strength (J/m)	25	38	109	14	N/A
Flexural modulus (GPa)	2.2	1.6	0.82	3.3	3.7
Tensile strength (MPa)	65.0	55.7	31.8	51.1	75.2
Tensile modulus (GPa)	2.80	2.80	1.26	3.60	4.10
Elongation at break (%)	6.2	24	49	2.0	5.6
HDT @ 0.45 Mpa (°C)	73	48	43	289	88

1.2. Tribology

The history of tribology dates back to the Prehistoric Epoch (until 3500 B.C.), also known as the Stone Age [16]. From there, tribology progressed to stone sockets and sliding bearings during the early civilization, gears, first designs of roller bearings, and lubricant development during the Greek and Roman epoch (900 B.C. – 400 A.D.), and then making rapid progress (involving development of complicated machine elements, gears and lubrication systems) during and after

the Industrial Revolution[17]. Specially in the Renaissance era, there was significant progress involving discovering fundamental tribological laws and correlations.

The term ‘tribology’ was formed by a working group formed by the Ministry of State for Education and Science in England, in 1966[18]. The word “tribology” is derived from two Greek words, ‘tribos’ meaning rubbing and ‘logos’ meaning study[19]. The British Lubrication Engineering Working group defined tribology as “the science and technology of interacting surfaces in relative motion and of related subjects and practices” [20]. Wear, friction and lubrication are three important parts of any tribological analysis.

Most mechanical systems involve some sort of sliding or rolling mechanism, and as such tribology is therefore an important technology with a wide range of applications[21]. Tribological analysis of moving systems is of significant economic importance and applies to diverse fields such as bioengineering, manufacturing, memory device technology, space engineering, nanodevices etc.

The field of tribology is broader than just a frictional analysis of systems, however friction does play a very important role. Based on the implementation, the effect of friction might be either positive or negative. In some cases, low values of friction are desired, for examples, door hinges, human joints or structural supports. In applications such as gears and bearings in mechanical systems, the work done in overcoming friction is dissipated as heat, and hence by reducing friction the overall efficiency of the system can be significantly increased. In other cases, high friction values are desired and even essential[21]. For example, in brakes and clutches, sufficient

and controlled friction is essential to efficiently dissipate kinetic energy and transfer torque; similarly, adequate friction is required between the human foot and ground to allow us to walk properly, just as adequate friction is required between a vehicle tire and the road surface for a car to be able to move.

Wear is another important constituent of tribology. Wear takes place when two or more surfaces move over each other leading to incresaing loss of material. In most cases, wear is damaging and undesirable, leading to greater clearances between moving parts, loss of precision, increased mechanical loading, and in severe cases fatigue failure and machine breakdown. Even relatively small amounts of wear can lead to mechanical failure of large machines. There have been a large number of cases where major engineering failures have been traced back to wear. On the other hand, in some applications high wear rates may be desired. For example, grinding and polishing are processes commonly used in the manufacturing industry for controlled removal of material using wear, and an initial small amount of wear is often expected and even desired during the running-in process of some kinds of machinery[21].

The third important constituent of tribology is lubrication – the process of using a lubricant (such as oil or grease) to reduce friction and wear between surfaces in contact. The study of lubrication is intricately linked with that of friction and wear. Artificial lubricants may be often added to systems to reduce friction and minimize wear[22]. Even when no artificial lubricants are used, atmospheric components (such as oxygen and water vapor in air) often play an identical role and hence it is important to consider their impact when studying the interaction of different surfaces[23].

1.2.1. Friction

Friction is the force that resists the relative motion of surfaces moving over one another, and this may include solid surfaces as well as fluid layers[24]. Friction usually involves two principal types of relative motion: sliding and rolling. Although sliding and rolling friction are different and distinctive, they are not mutually exclusive, 'pure' rolling almost often involves some sliding[24].

The value of the frictional force is usually expressed using the coefficient of friction. According to Coulomb-Amontons law, the coefficient of friction is a dimensionless number and is expressed as the ratio of the force to the normal load [26]. The value of the coefficient of friction usually varies from about 0.001 for low-friction applications (such as a lightly-loaded bearing) to greater than 10 for high-friction applications (such as brake pads). Usually for most common applications, (involving sliding in air and without any lubrication) the value of μ usually varies between 0.1 and 1[25].

Friction leads to energy dissipation and wear of material elements. The friction force between two mating surfaces depends on a multitude of factors including geometry, elastic properties, macroscopic contact points, adhesive forces, deformation and grooving of surfaces during movement etc.[25]. The different types of friction are[26]:

1. Sliding Friction – generated by sliding contact, without any rolling and/or spin.
2. Rolling Friction – generated by rolling contact.

3. Static Friction – occurs when objects are resting on each other. It is defined as the coefficient of friction corresponding to the maximum force that must be overcome to initiate macroscopic motion between contacting surfaces (ASTM).
4. Kinetic Friction –occurs due to relative motion between mating surfaces. It is defined as the friction coefficient under conditions of macroscopic relative motion between two bodies. It is also known as the dynamic coefficient of friction.
5. Stick-slip –occurs from extremely low-speed sliding movements when the mating surfaces are connected to a vibrating system. Stick-slip friction is usually found in machine tools operating with slow feeds, often leading to chatter marks on components.

1.2.2. Wear

As per the German DIN standard 50 320, wear is defined as "the progressive loss of material from the surfaces of contacting bodies as a result of mechanical causes". It has been estimated that the wear of mechanical components costs the US economy between 6-&% of the gross national product[27]. Therefore, it is of critical importance to have an in-depth understanding of the wear process and wear mechanisms in order to implement effective control measures.

There are various factors that affect the rate of wear, some of the more important ones include loading, speed, type of contact, lubrication, type of environment etc.[28]. Wear can be measured using a number of different approaches - gravimetrically, volumetrically or in terms of area over a period of time or against increasing load[26].

Some of the common wear mechanisms are listed below:

1. Adhesion – Considered one of the most complex wear mechanisms, adhesion takes place when molecular and atomic interactions between the mating surfaces remove/shred material particles away from the contact surfaces. This is preceded by a phenomenon called cold welding, which involves a spot joint formation between the mating surfaces. Micro spot shearing is an important aspect of adhesive wear[26].
2. Abrasion –caused due to the sliding of the asperities of a rough, hard surface on a softer surface. This leads to interfacial damage due to plastic deformation and/or fracture[23].
3. Erosion – In erosion wear, material is lost from the surface of a solid due to the impingement of the surface by a fluid containing solid particles.
4. Tribochemical reactions – Tribochemistry refers to the chemical reactions that occur in tribological conditions. The transfer/expulsion of the reaction layers produced from these tribochemical reactions constitute tribochemical wear[22].
5. Surface Fatigue – Caused due to periodic loads in the contact zones of the mating surfaces. Such recurrent spot loading causes material fatigue, and this in turn leads to surface fatigue[23].
6. Cavitation – Cavitation takes place due to imploding gas and vapor bubbles entrained in lubricating oils or hydraulic fluids leading to material removal and material loss. In lubricated systems, eliminating entrained air, substances with low boiling points, or using surface-active components, can help such gas/vapor bubbles, thereby controlling and reducing cavitation[27].
7. Fretting – Fretting takes place at the contact region between two mating surfaces under load. It may be caused due to vibration, relative motion, or some other force. Relative motion between the mating surfaces leads to adhesive wear and production of debris, this

debris then gets oxidized to form hard particles thereby causing abrasive wear at the contact surfaces, leading to localized damage, deformation, grooving and loss of contact[28].

1.3. Polymer-based nanocomposites

Polymer-based composites are widely used in the industry and in a wide range of applications including but not limited to damping elastomers, thermal/electrical conductors, and high-performance composites for use in automobiles and aircrafts. When creating a polymer composite, synergistic materials are selected to design composites with specific customized properties. However, in spite of tremendous optimization, traditional micrometer-scale composite fillers have certain limitations, the most important of which is that the enhanced properties usually involve compromises. For example, stiffness might be traded for hardness, or hardness for optical clarity. Alongside, the filler volume fraction (high or low) may cause macroscopic defects ultimately leading to failure or breakdown[29].

Most of these limitations, faced by traditional micrometer-scale polymer composites, can be overcome by nanoscale-filled polymer composites – where the size of the filler is < 100 nm in at least one dimension. Several studies have shown that nanocomposites exhibit superior mechanical, electrical and thermal properties as compared to traditional composites. As compared to the low density of the polymer matrix, micrometer filler exhibit relatively high density. As a result, a large amount of filler is required for performance improvement, which in turn increases the weight of the composite. This is not the case with polymer nanocomposites, which possess the unique

capability to provide significant performance improvement at low filler content. This in turn allows the nanocomposites to be lightweight.

Due to the tiny size of the nanofillers, often the particles exhibit unique properties and behavior. Moreover, the small size of the fillers results in a significantly large interfacial area in the composites, which in turn enhances the interaction between the nanoparticles and polymer matrix, leading to enhanced properties. Two of the biggest challenges in developing polymer nanocomposites are achieving good dispersion of the nanoparticles in the polymer matrix, and controlling the interface in order to achieve optimal properties.

Depending on the physical and chemical characteristics of the base polymer, different nanoparticle additives may offer different degrees of performance improvement in different areas (mechanical, electrical and/or thermal properties). The degree of performance enhancement is governed by the compatibility between the polymer and the nanoparticle additive, structure & morphology of the nanoparticles and several other factors. The below table shows a comparison of the degree of performance improvement of the mechanical properties of nanofiller/polylactic acid composite nanofiber membranes, gathered by different published studies[30]:

Table 2. Comparison of mechanical properties of nanofiller/PLA composite nanofiber membranes

Matrix polymer	Nanoparticle	Nanoparticle weight fraction (%)	Tensile strength improvement (%)	Young's modulus improvement (%)	References
PLA	MWCNT	1.3	94	153	[31]
	Tricalcium phosphate	20	-142	-	[32]
	Nanohydroxyapatite	5	200	12	[33]
	Al_2O_3	1	-	38	[34]
	Al_2O_3.Ag	25	228	-	[35]
	ZnO	1	38	142	[36]
	Nanodiamond	1	239	161	[30]

Having a high surface-to-volume ratio, nanoparticles have been found to impart a number of unique and enhanced properties as compared to the bulk material[37]. Researches in the field of polymer nanocomposites have shown that nanoparticles show tremendous potential in the field of tribology as additives. Addition of nanoparticles as additives has shown to increase friction resistance[38], wear resistance [38] and load bearing capacity of engine oil[39]. One of the primary reasons for this performance enhancement is the ability of nanoparticles to embed themselves in the small surface asperities and thus reducing the actual contact area of the mating surfaces which

in turn leads to reduced wear at the contact surfaces. Various nanoparticles such as copper [40], molybdenum disulphide [39] , palladium [31] etc. have proven to exhibit

enhanced anti-wear, anti-friction and load bearing capabilities than conventional lubricants such as ZDDP available in the market.

Table 3. Friction and wear performance of polymer nanocomposites

Matrix/ Nanoparticle	Nanoparticle size(nm)	Content for optimal wear performance (vol. %)	Change in COF	Minimum wear rate (10^{-6} mm^3/Nm)	Wear rate of pure polymer (10^{-6} mm^3/Nm)	References
PEEK/SiC	<100	1.06-4.4	Decrease	3.4	7.4	[41]
PEEK/ZrO_2	10	1.8	Decrease	3.9	7.4	[42]
PPS/Al_2O_3	33	2	Increase	12	23	[43]
PPS/TiO_2	30-50	2	Decrease	8	16.6	[40]
PTFE/ZnO	50	15	Minor	13	1125.3	[36]
PTFE/Al_2O_3	40	1	Increase	1.2	715	[44]

1.4. Zirconium Phosphate nanoparticles

Layered zirconium hydrogen phosphate with α-type structure, $Zr(HPO_4)_2.H_2O$ is an important inorganic material used in diverse applications such as, heterogeneous catalyst, ion exchanger,

nanocomposite formulations, intercalating agent, drug delivery and immobilization of biological materials, and proton conductor for fuel cells[45]. It has been shown in previous studies that the morphology of ZrP nanoparticles show hexagonal plates, in which the disks have well-defined shapes with very smooth surfaces, with parallel solid layers showing good crystallinity[46].

In recent studies, the addition of α-ZrP nanoparticles into pure base oils showed a significant improvement in friction and wear performance[47]. Amine intercalated α-ZrP nanoparticles used in a mineral oil reduced friction by more than 60%[46]. Another study involved experiments on a base oil containing 0.2 % by weight of the α-ZrP nanoparticle additives. The results showed a 50% improvement in friction performance (reduction in friction coefficient) and a 30% improvement in wear performance when compared to the base oil containing 0.8 % by weight of ZDDP, a commercially used additive[48]. From investigations of the concerned tribofilm, it was found that the sheet-like morphology of the α-ZrP nanoparticles were a key factor in improving the friction and wear performance. The two-dimensional nature of the nanoparticles allowed them to enter into the space between the mating surfaces in the boundary lubrication regime. Also, the relatively large size of the nanoparticles on the disk surface allowed them to efficiently carry a load. This along with weak van der Waals force led to a shear force[48]. It was concluded that the zirconium based tribofilm exhibited low surface roughness values and provided an enhanced load bearing capability thereby enhancing friction and wear performance.

In this research α-ZrP nanoparticles have been selected as additive over other materials (such as MoS_2 and graphite) because:

- α-ZrP is an eco- friendly, anti-wear additive.
- Sheet-like morphology of α-ZrP nanoparticles is particularly effective in reducing friction and improving wear performance[38].
- Compared to conventional layered materials, such as MoS_2 and graphite, α-ZrP is a low-cost synthetic material. Moreover, its particle size and product quality can be easily controlled by the controlling the different synthesis conditions[39].

Table 4. Friction and wear performance of α-ZrP over other nanoparticles (MoS_2 and graphite) for vegetable oil and white oil grease samples at 600 N. Reprinted from [39].

Oil	Nanoparticle Additive	Nanoparticle Size (nm)	Wear Volume (× 10^{-4} mm^3)	Mean Friction Coefficient
Castor oil	α-ZrP	50-100	5.7	0.110
	MoS2	50-100	22	0.113
	Graphite	100-200	18.3	0.118
Coconut oil	α-ZrP	50-100	5	0.101
	MoS2	50-100	38	0.909
	Graphite	100-200	22	0.106
White oil	α-ZrP	50-100	5.3	0.097
	MoS2	50-100	35	0.126
	Graphite	100-200	34	0.123

1.5. Summary

As discussed in this chapter, the SLA market, is expanding rapidly. The main limitation holding back the SLA printing industry is the limited number of commercially-available high-performance resins. Nanoscale filled polymer composites have proven to exhibit superior mechanical, electrical and thermal properties as compared to traditional composites. However, not much work has been done exploring the viability of using nanoscale additives in SLA printing. This research intends to explores the development, synthesis and tribological evaluation of novel photoactivated polymer nanocomposites for SLA printing purposes.

α-ZrP is an inexpensive, environmentally friendly anti-wear additive that has been shown to improve friction and wear performance. However, to evaluate the viability of α-ZrP nanoparticles for divergent tribological applications further studies need to be performed. In this study, we intend to carry out the design, synthesis and tribological evaluation of a ZrP-based polymer nanocomposite for stereolithographic printing applications. This research explores the compatibility of using α-ZrP nanoparticles as fillers with standard SLA resin for 3D printing, and examine the tribological performance of the 3D printed parts. The final goal is to develop a cost-effective novel photoactivated polymer nanocomposite for use with SLA printing that exhibits superior tribological performance.

CHAPTER II

MOTIVATION & OBJECTIVES

As discussed in Chapter I, stereolithography (SLA) technology is the most accurate (commercially-available) form of 3D printing and the third most popular 3D printing technology. The main limitation of the SLA process is considered to be the limited number of commercially-available high-performance resins. This is where our research adds tremendous value. In this research we conduct the design, synthesis and tribological evaluation of polymer-based 3D printable photoactivated nanocomposite using α-ZrP nanoparticles as the nanofillers.

As discussed in Chapter I, in previous studies, α-ZrP nanoparticles have been shown to improve the friction and wear performance in a mineral oil as well as in a commercial-based oil. In this study, we further investigate the effects of using α-ZrP nanoparticles as nanofillers, in terms of tribological performance enhancement, for the development & synthesis of a polymer-based 3D printable photoactivated nanocomposite. The wear & friction behaviors of the pure polymer and the polymer nanocomposite will be compared to evaluate the performance change. The knowledge gained from this study will greatly aid the design of a novel photoactivated polymer nanocomposite for SLA that can be used to fabricate parts exhibiting superior tribological performance.

The goal of this research is to obtain an understanding of the role of α-ZrP nanoparticles in the design and synthesis of high-performance photopolymer resins for SLA printing. The overall

approach is illustrated in Figure 3. We start with designing a photopolymer nanocomposite using standard clear resin as the polymer matrix and α-ZrP NPs as the additives. In the next step, we use two distinct approaches to fabricate samples – casting versus 3D printing. The fabricated sample are subject to tribological evaluation - friction and wear tests. After tribo-characterization, the surfaces of the tested samples are analyzed to characterize wear morphology, evaluate wear rate, and understand the underlying wear mechanisms. Finally, the research data is used to propose a novel 3D printable photopolymer nanocomposite for advanced manufacturing.

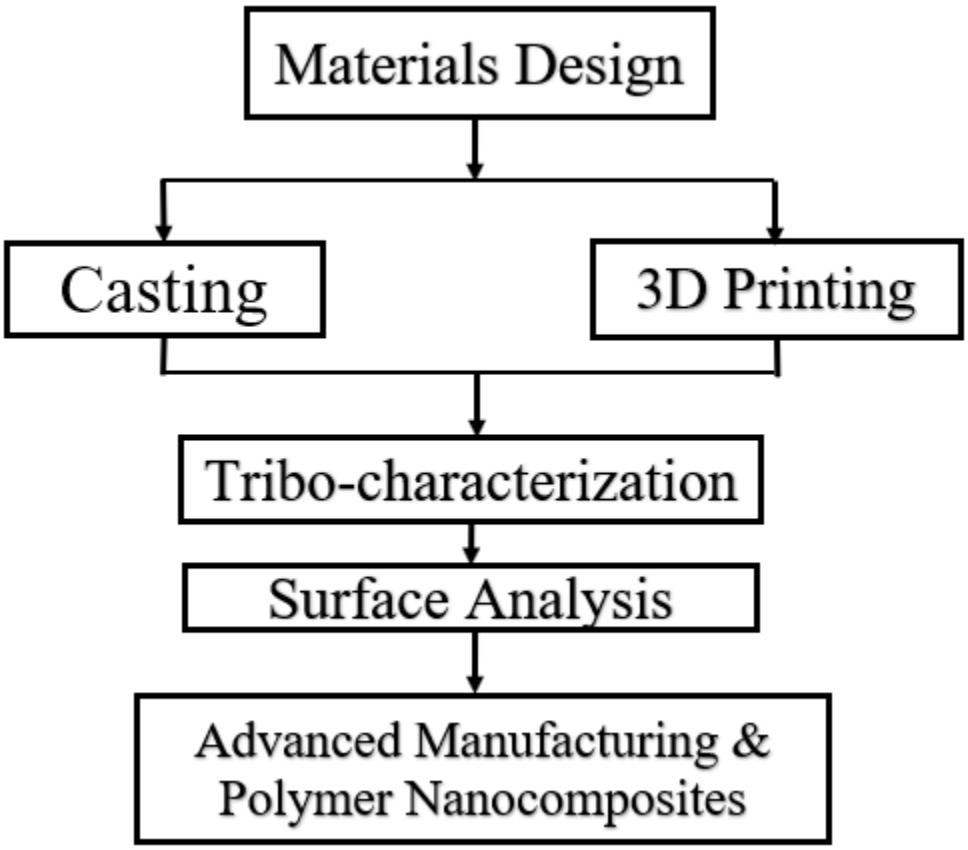

Figure 3. Research Flowchart

The objectives for this research may be summed up as follows:

1. Investigate the viability of using α-ZrP nanoparticles as nanofillers for SLA printing.

2. Design and synthesize a novel photopolymer nanocomposite (using α-ZrP nanoparticles as nanofillers) for SLA-printing.
3. Conduct a comparative analysis of the SLA-printed parts fabricated (pure photopolymer verses nanocomposites) to evaluate performance change.
4. Perform a tribological evaluation of the 3D printed photopolymer nanocomposites.

The findings of this research will be beneficial to the 3D printing industry as well as the polymer nanocomposite industry, and will open up new arenas for the use of nanoparticle additives in SLA printing for fabricating high performance polymer-based photoactivated nanocomposites.

CHAPTER III

EXPERIMENTAL DETAILS

This chapter discusses the materials and experimentation methods used in this research. It includes materials, sample preparation methodologies, tribometer experiments, wear & friction analysis, and wear surface characterization. The first section discusses the nanoparticles and photopolymer used in this research - α-ZrP and MoS_2 nanoparticles, and Formlabs Standard Clear Resin. This is followed by discussing the sample fabrication approaches used in this research – manual curing and 3D printing. After that, the tribometer experimentation methodology is explained. Finally, the study of the effects of α-ZrP nanoparticle additives on the wear and friction performance of the novel photopolymer nanocomposite is conducted by performing frictional analysis, wear analysis, wear surface characterization, and wear rate evaluation. For wear surface characterization and wear rate evaluation, optical microscopic and interferometric data have been used in this research.

3.1. Materials

Nanoparticles have been extensively used as additives to develop polymer nanocomposites with enhanced tribological properties. Various studies have been conducted studying the positive effects of α-ZrP nanoparticle additives on the friction and wear performance of liquid and solid lubricants[46-48]. This research focuses on designing, synthesizing and conducting the tribological evaluation of a novel photopolymer nanocomposite using Formlabs Standard Clear Resin as the photopolymer and α-ZrP nanoparticles as the additive.

3.1.1. Zirconium phosphate nanoparticles

Layered zirconium hydrogen phosphate with an α-type structure, $Zr(HPO_4)_2.H_2O$, is a two-dimensional layered structured material with a lamellar crystal structure and high surface energy[49]. It has been observed that the interaction between the hydrogen bonds of two adjacent layers of ZrP is greater than those in 2D nanomaterials with van der Waals bonding[38]. α-ZrP nanoparticles exhibit quite a few unique characteristics, such as high thermal and chemical stability, ionizing radiation resistance, and ion conductivity in solid state[50].

Depending on the crystalline structure and inter-laminar spaces, zirconium hydrogen phosphate may exhibit different phases. Among the various phases, the alpha phase $Zr(HPO_4)_2.H_2O$ and the gamma phase $Zr(PO_4).(H_2PO_4).H_2O$) are the most extensively used ones. α-ZrP has been used in this research to synthesize a novel photoactivated polymer nanocomposite.

Layered zirconium hydrogen phosphate with α-type structure, $Zr(HPO_4)_2.H_2O$ can be synthesized using several different methods including hydrothermal method, refluxing method, and HF method[49]. By controlling the temperature, pressure, concentration of reactants, and using a complexing agent, the aspect ratio of the nanoparticles can be easily controlled[49]. In this research, the hydrothermal method was used to synthesize the α-ZrP nanoparticles. The nanoparticles obtained resembled the shape of nanoplatelets with 600 nm ± 400 nm in width and 19 nm ± 11 nm in height. The TEM and AFM images of the NPs synthesized using the hydrothermal method is provided in figure 4.

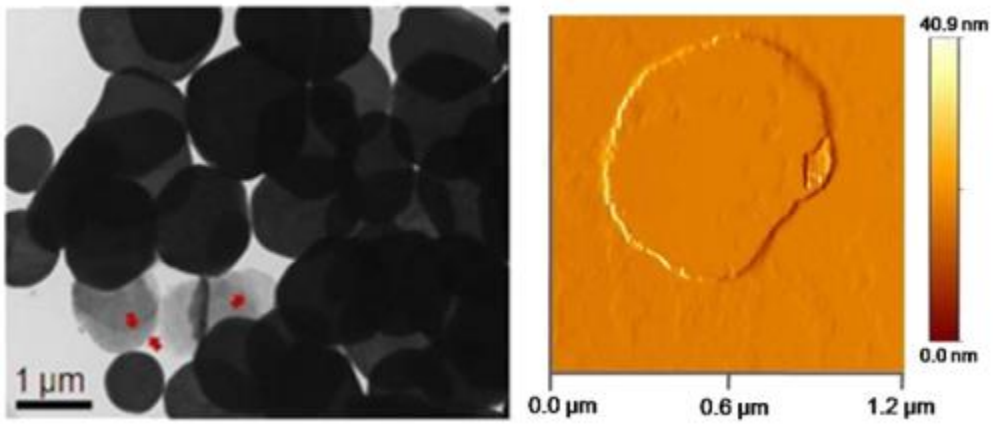

Figure 4. TEM (left) and AFM (right) images of α-ZrP nanoparticles. Reprinted with permission from [47].

3.1.2. Molybdenum disulphide nanoparticles

Molydbneum disulphide is a well-known anti-wear additive and is a common lubricant additive. Similar to α-ZrP, MoS_2 nanoparticles also have a two-dimensional layered structure. They exhibit strong interlayer covalent bonds and weak van der Waals forces between molecular layers[51]. MoS_2 nanoparticles have been shown to be effective in reducing friction in the boundary-layer lubrication of steel-steel contacts and titanium-steel pairs by forming a conformal protective tribofilm on the sliding contact interfaces[52-54]. Studies have also shown that MoS_2 nanoparticles can efficiently reduce friction on relatively inert surfaces, such as diamond-like carbon coating[55, 56]. The tribological performance of MoS_2 nanoparticles depends on several factors such as quantity, morphology, size, crystal structure, as well as the nature of the contact surfaces[57].

Because of its layered structure, MoS_2 nanoparticles are commonly used as a solid lubricant. MoS_2 nanoparticles exhibit unique properties such as excellent friction performance, large active surface area, enhanced adsorption capacity, high reactivity and catalytic properties. Studies have shown that decrease in size of MoS_2 nanoparticles significantly improve anti-wear and anti-friction properties[57].

The MoS_2 nanoparticles used in this research were purchased from XYZ Company. The nanoparticles obtained were 400 nm ± 200 nm in width and 30 nm ± 10 nm in height. In this research, the tribological performance of α-ZrP photopolymer nanocomposite is compared against that of MoS_2 photopolymer nanocomposite, while keeping all factors such as nanoparticle concentration, photopolymer substrate and curing parameters unchanged.

3.1.3. Clear Resin for SLA Printing

In this research, a standard SLA clear resin is studied as the photopolymer. Clear resin is a low-cost methacrylate resin that provides high stiffness and allows for high-resolution prints. Parts printed using standard clear resin exhibit a smooth injection-molding finish and as such they are ideal for concept modeling, prototyping applications, and for showcasing internal features. Using post-processing, these parts can be developed to near optical transparency.

Formlabs Standard Clear Resin is the recommended clear resin for use with Formlabs 3D printers. It is a liquid photoreactive resin consisting of a mixture of methacrylic acid esters and

photoinitiator[58]. Clear resin contains derivatives of methacrylic acid including the parent acid ($CH_2C(CH_3)CO_2H$), and esters such methyl methacrylate ($CH_2C(CH_3)CO_2CH_3$)[59].

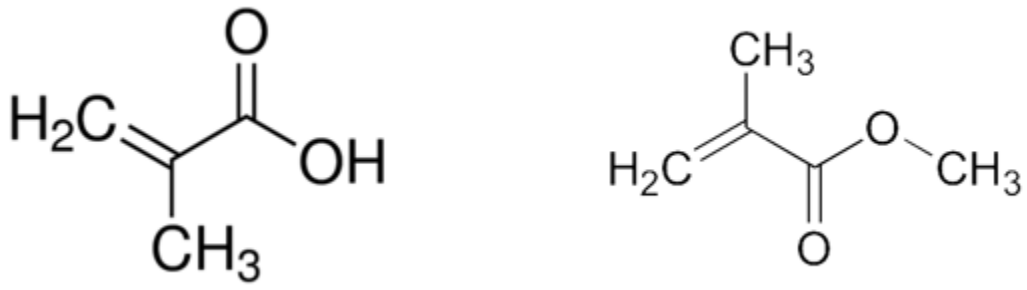

Figure 5. Chemical structure of Methacrylic acid (left) and Methyl Methacrylate. Reprinted from [59].

Table 5. Composition of Standard Clear Resin. Reprinted from [58]

Product/Ingredient Name	% (by volume)
Methacrylated oligomer	≥ 75 - ≤ 90
Methacrylated monomer	≥ 10 - ≤ 25
Diphenyl (2,4,6-trimethylbenzoyl) phosphine oxide	< 1

Table 6 lists some of the important mechanical properties of parts printed using Formlabs Standard Clear Resin. It is to be noted that material properties of printed parts depend on several factors

such as orientation of the part on the build platform, geometry of the part, temperature and print settings.

Table 6. Common mechanical properties of parts printed using Clear Resin. Reprinted from [60]

Property	Without post cure	Post-Cured
Ultimate Tensile Strength	38 MPa	65 MPa
Tensile Modulus	1.6 GPa	2.8 GPa
Elongation at break	12%	6%
Flexural Modulus	1.3 GPa	2.2 GPa
Notched IZOD Impact Strength	16 J/m	25 J/m
Heat Deflection Temp.@ 1.8 MPa	42.7°C	58.4°C
Heat Deflection Temp.@ 0.45 MPa	49.7°C	73.1°C

In Table 6, data for parts without post-curing were obtained from green parts printed using Form 2 3D printer using a resolution of 100 μm with "Clear Resin" settings. After printing the parts were rinsed in isopropyl alcohol and air dried, without post cure. Data for parts with post-curing were obtained from parts printed using the same resolution and settings as the green parts. However, these parts were post-cured with 1.25 mW/cm^2 of 405 nm LED light for 60 minutes at 60°C.

3.2. Sample Preparation

3.2.1. Synthesis of polymer nanocomposite

In order to achieve optimal properties, it is important to ensure optimal dispersion of nanoparticles in the polymer matrix. Several techniques are available to introduce nanoparticles into a polymer matrix. The different mixing techniques facilitate uniform dispersion of nanoparticles from agglomerated state into a homogeneous state. In this study, magnetic stirring and ultrasonic mixing methods have been used to ensure proper dispersion of nanoparticles in the polymer matrix.

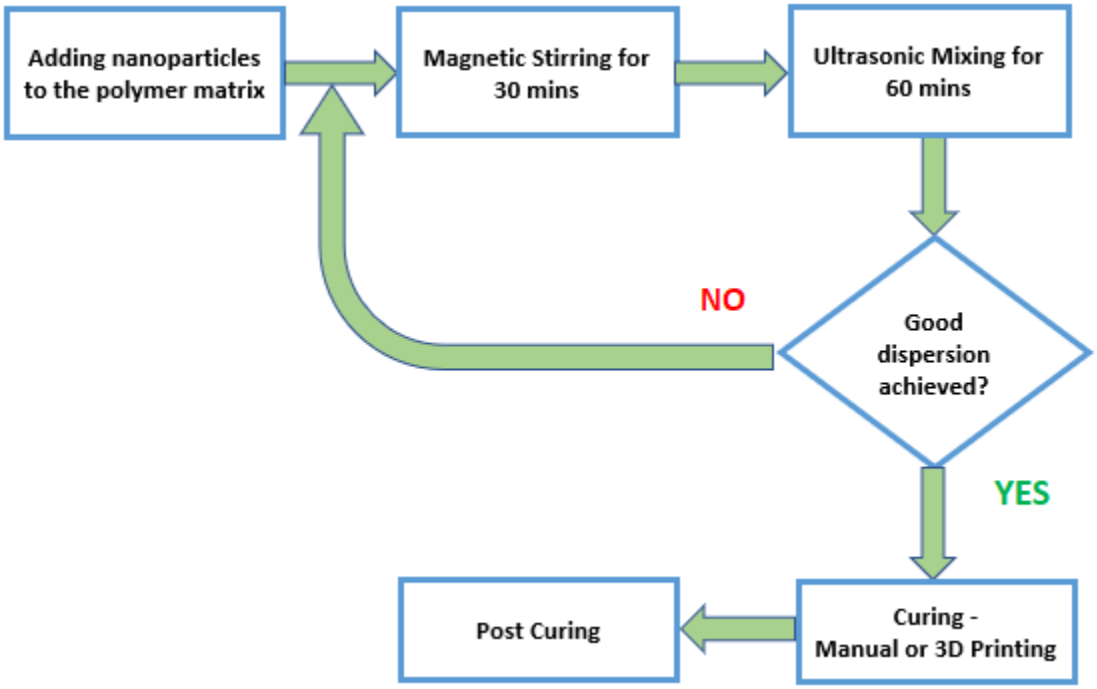

Figure 6. Block diagram showing the different processes involved in sample preparation

A known quantity of nanoparticles (0.1% - 1% by weight) is mixed with the Formlabs Standard Clear Resin. To achieve proper dispersion, the mixture is first stirred using a Corning PC-353 Magnetic Stirrer for 30 minutes. This mixture is then mixed using a Bransonic B-220 ultrasonic mixer for 60 minutes in order to achieve a homogeneous dispersion. The mixture is then visually

inspected to ensure good dispersion of nanoparticles in the Clear Resin polymer matrix. In case, some nanoparticle agglomerations are still visible, the mixture is again subjected to another round of magnetic stirring followed by ultrasonic mixing, until a homogeneous dispersion is achieved.

Figure 7. Corning PC-353 Magnetic Stirrer

Figure 8. Bransonic B-220 Ultrasonic Mixer

3.2.2. Sample fabrication

Once the polymer nanocomposite mixture is synthesized, it is subjected to curing to produce the sample for tribological evaluation. In this study, two different approaches have been used in this regard, which are discussed in detail below.

1. Curing

   In this method, the polymer nanocomposite mixture is manually cured using a 405 nm wavelength UV light. A picture of the setup is provided below in Fig. 9.

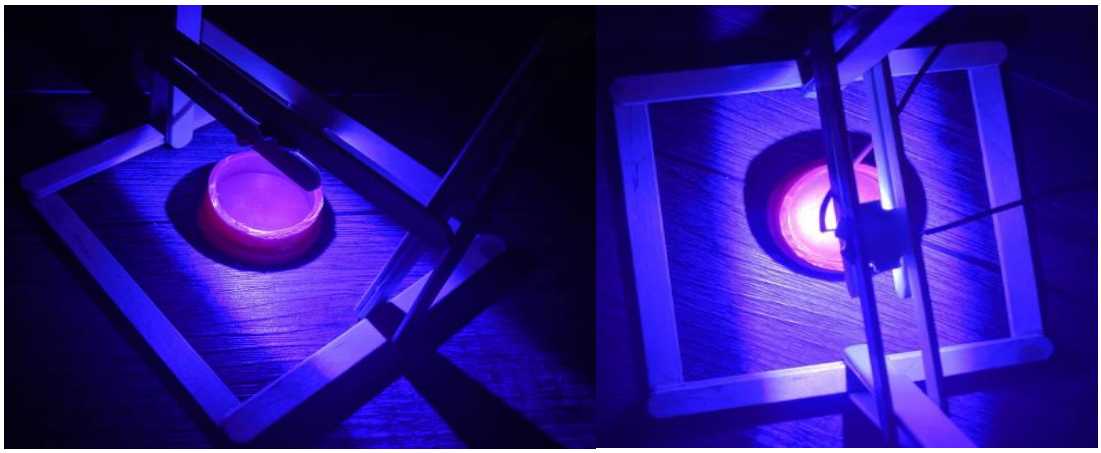

Figure 9. Setup for manual curing of photopolymer nanocomposite

The setup consists of a 3-W high power LED chip, emitting 405 nm UV light with an emitting angle of 120-140°, supported on a wooden frame constructed using ice cream sticks. The LED chip is mounted on a heatsink to prevent the system from overheating. The wavelength of UV light used in this method is the same as that provided in Formlabs Form 2 3D printer.

The volume of each sample (for curing) is kept between 4-5 ml. The liquid polymer nanocomposite is poured into the plastic mold and subjected to a curing for 3 hours. After curing, the printed samples are soaked in an alcohol bath (containing isopropyl alcohol) for 10 minutes to remove any liquid resin from the exterior surfaces. After rinsing, the samples are taken out of the alcohol bath and let to air dry. If the sample surface is found to be uneven, the surface is polished and made even using 120, 360 and 600 grit sand paper.

Figure 10. Sample printed using manual curing

2. 3D Printing

In this method, a Formlabs Form 2 3D printer is used to print the samples, using the polymer nanocomposite mixture previously synthesized.

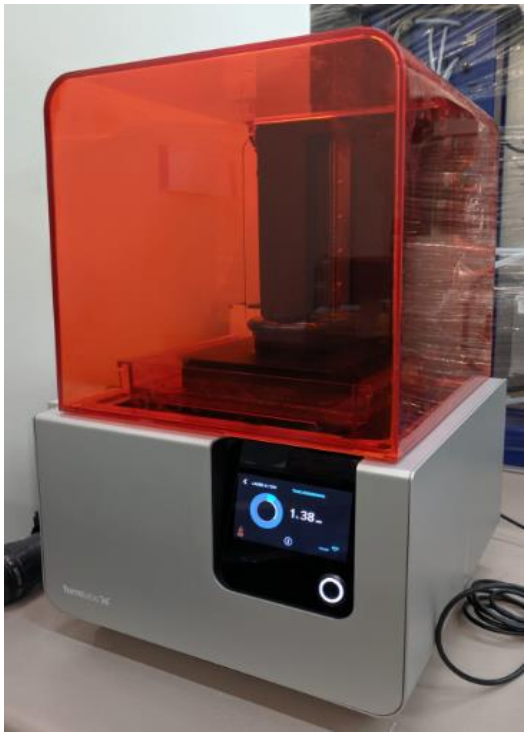

Figure 11. Formlabs Form 2 3D Printer

A cylindrical disc, having radius 15 mm and height 3 mm, is designed using SolidWorks and exported into a STL file. This STL was then imported into the PreForm print preparation software. All samples are printed with 100 μm resolution and "Clear Resin" settings. The 3D printer is run on "Open Mode" using the polymer nanocomposite mixture.

Once the printing process is completed, the 3D printed part is removed the printer and soaked in an alcohol bath (containing isopropyl alcohol) for 10 minutes to get rid of any liquid resin from the exterior surfaces. After rinsing, the samples are taken out of the alcohol bath and let to air dry.

Figure 12. 3D Printed Sample

3.3. Tribometer Experimentation

In this study, a pin-on-disk tribometer is used to carry out friction and wear tests at room temperature, to evaluate the tribological properties of the different samples.

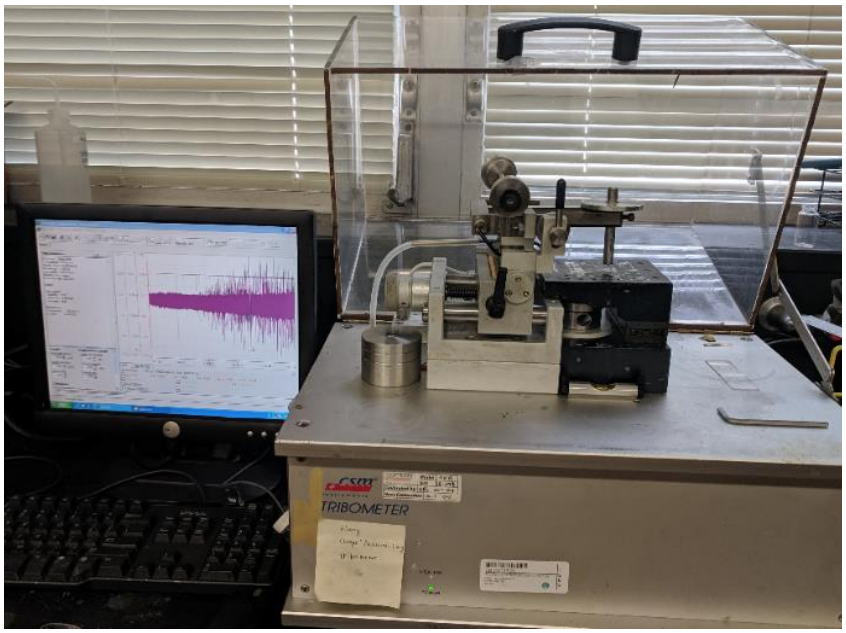

Figure 13. Pin-on-disc tribometer

The pin-on-disc tribometer setup is shown in Fig. 13 The tribotester consists of a pin, a 7 mm diameter (D521000) stainless-steel ball bearing, a measurement arm, a disc with spindle motor. A computer with the Tribo X software is connected to the tribotester to capture data from the instrument. The tribometer can be run in two different modes – rotating mode and reciprocating mode. In this study, we have used the reciprocating test mode to conduct friction and wear tests.

The elastic arm of the tribometer maintains a nearly fixed contact point and a stable position in the friction track, formed by the stainless-steel ball on the sample. Using the Tribo X program, data is gathered from the tribometer tests in real-time. After running a test, this data can be saved and extracted for further analysis. During a friction test, the kinetic coefficient of friction is determined by measuring the change in torque through a sensor located at the pivot point of the arm.

In this study, all samples are subjected to friction and wear tests in reciprocating test mode, under a 1 N, load at a linear speed of 5 cm/s and over a distance of 1000 m. The sliding distance is set to 5 mm for all tests.

3.4. Wear Analysis

To calculate the wear volume, wear rate and characterize the wear morphology, interferometry and optical microscopy have been used in this research.

3.4.1. Interferometer

Interferometer is an instrument that creates an interference pattern by merging two or more sources of light. The data captured from this interference pattern contains information about the surface or phenomenon being studied[61].

In this study we use an optical interferometer to characterize the wear surface, as well as to measure the wear track depth and surface roughness. In an optical interferometer, a beam of light divides into multiple beams which travel different lengths and on reuniting, their intensities create an interference pattern. This appears as a pattern of light and dark bands called interference fringes[62]. The data captured from these fringe measurements can be utilized to determine surface irregularities, measure surface roughness and surface topography.

The figure 14 shows the optical surface interferometer used in this research. This 3D optical surface interferometer uses scanning white light interferometry to image and evaluate the surface morphology. It has three objectives, including 10-, 20- and 50-times magnification. Depending on the objective, 2D and 3D images of certain resolution were captured to determine surface roughness values and wear track depth. 10-times and 20-times objective images have been used in this research, to compute wear track depth and evaluate wear track morphology.

Figure 14. Zygo New View 600 Optical Interferometer

3.4.2. Optical Microscope

The optical microscope that uses visible light and a system of lenses to magnify images of specimens under investigation[63]. They are designed to create magnified images (visual or photographic) of small objects. An optical microscope achieves this objective by:

1. Creating a magnified image of the sample.
2. Discerning different details of the image.
3. Making the final image visible to the human eye or camera.

Optical microscope, the oldest microscope, was possibly designed in its compound form at the beginning of the seventeenth century[64]. Optical microscope designs can vary from very simple to highly complex, depending on the resolution and sample contrast desired. Originally, optical microscopes used photographic films to capture images, but in recent years, developments in the area of complementary metal-oxide-semiconductor and charge-coupled-device (CCD) cameras has led to the use of digital imaging[63]. The purely digital microscopes, available in the market now, use a CCD camera for sample examination and show the resulting image directly on a computer screen.

Figure 15. Olympus PMG-3 Optical Microscope

In this study, we used an Olympus PMG-3 Optical Microscope (shown in Fig. 15) to capture microscopic images of the wear tracks. The Olympus PMG-3 uses a 12 V 100 W halogen lamp along with a CCD camera to capture digital images of the samples. The optical microscope is used at 10-, 20- and 50-times magnification to capture images of the worn surfaces. The magnified images are used in characterizing the wear as well as to measure the width of the wear track.

3.4.3. Wear Rate Evaluation

In this study we have used wear volume to determine the wear rate for different specimens. Wear volume is calculated from the wear track depth, wear track length and wear track width as below:

$$\text{Wear Volume} = \text{Depth}_{\text{wear track}} \times \text{Width}_{\text{wear track}} \times \text{Length}_{\text{wear track}}$$

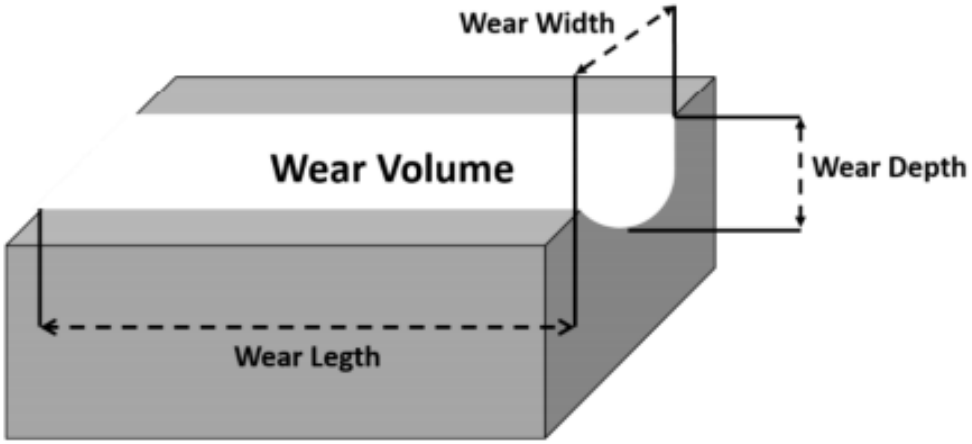

Figure 16. Wear volume calculation

Interferometry data has been used to evaluate the average wear track depth whereas optical microscopy data has been used to evaluate the average wear track width. The sliding distance value, set in the tribometer (during wear test), is used to compute the wear track length. After calculating these values, the wear rate is calculated using the below equation:

$$\text{Wear Rate } (\text{mm}^3/\text{N-mm}) = \frac{\text{Wear Volume (mm)}}{\text{Sliding Distance (mm)} * \text{Applied load (N)}}$$

CHAPTER IV

TRIBOLOGICAL EVALUATION OF CASTED PHOTOPOLYMER NANOCOMPOSITES

This chapter discusses the influence of α-ZrP nanoparticles on the tribological performance of casted clear resin samples. In the first segment, the influence of α-ZrP nanoparticles on the friction performance of clear resin is discussed. The effect of nanoparticle concentration on friction performance is studied by analyzing the variation of the kinetic coefficient of friction with nanoparticle concentration. Comparison is also made with the friction performance of MoS_2 embedded photopolymer nanocomposite.

In the second section, the effect of α-ZrP nanoparticles on the wear performance of clear resin is analyzed. Wear performance is studied with respect to wear rate and wear morphology. The effect of nanoparticle concentration on wear volume is studied by analyzing the change in wear volume with nanoparticle concentration. Comparison is also made with the wear performance of MoS_2 photopolymer nanocomposite. Finally, the effect of nanoparticle shape and morphology on the wear mechanism of α-ZrP photopolymer nanocomposite is examined in detail.

4.1. Frictional Behavior

In this study, the friction performance of casted specimens containing different concentrations of α-ZrP nanoparticles are studied. Five tribometer friction tests are conducted for each specimen to confirm repeatability of results. It is observed that for low concentrations of α-ZrP nanoparticles

(≤ 0.25%), there is a considerable reduction in the kinetic coefficient of friction (19% ≥ CoF ≤ 33%) at room temperature.

4.1.1. Effect of concentration

In this study, the concentration of α-ZrP nanoparticles is varied between 0.1% - 1% by weight and the friction performance of the polymer nanocomposites are examined. Specimens containing 0.1%, 0.25%, 0.5% and 1% α-ZrP nanoparticles by weight are subjected to reciprocating friction test using the pin-on-disc tribometer at room temperature. Friction data captured using the TriboX software is used to generate graphs showing the variation of friction coefficient with distance.

Figure 17 shows the friction behavior of the different casted samples. Specimens containing 0.1% and 0.25% α-ZrP nanoparticles by weight show a considerable performance improvement when compared with the friction performance of clear resin specimen (without nanoparticles). It is observed that as with the increase in concentration of α-ZrP nanoparticles the coefficient of friction also increases.

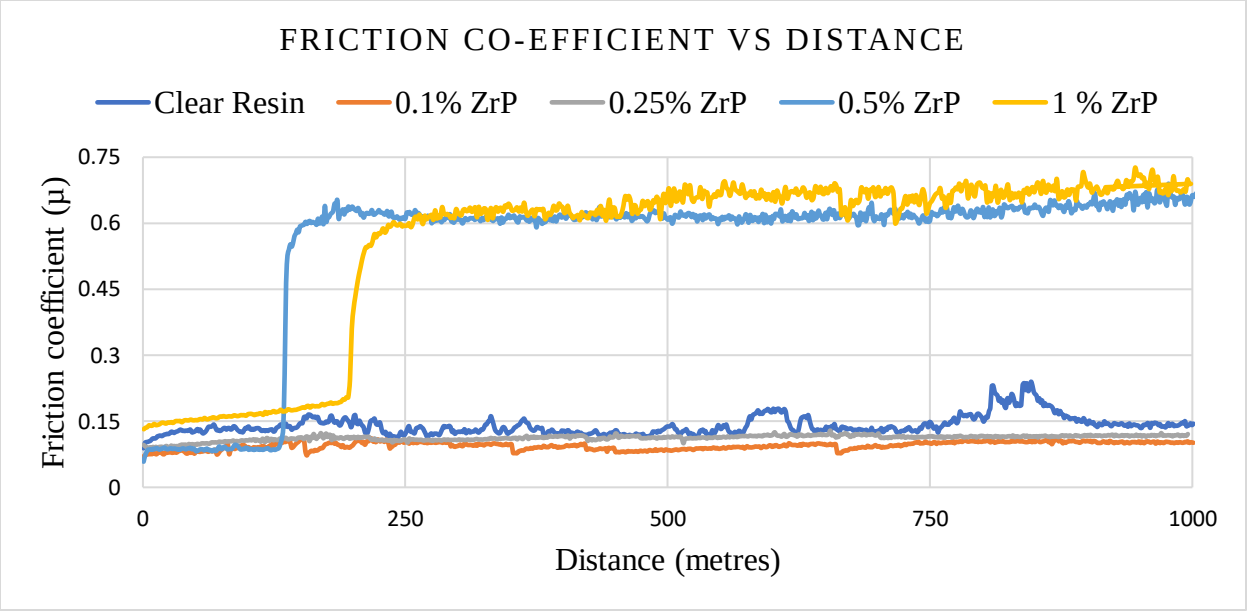

Figure 17. Friction data for casted samples containing different concentrations of α-ZrP nanoparticles (by weight)

Figure 18 compares the friction performance of pure clear resin sample with that of polymer nanocomposites containing 0.1% and 0.25% α-ZrP nanoparticles by weight. Optimal performance is obtained with the 0.1% α-ZrP nanoparticle concentration, showing a 32% decrease in friction coefficient when compared with the clear resin specimen (without additives). This result can be attributed to the disc-like shape of the nanoparticles, and the load-bearing capability of the nanoparticles at the contact region between the two mating surfaces. The disc-shaped nanoparticles enter into the spatial region between the mating surfaces and effectively carry a load, thereby decreasing the effective contact area of the mating surfaces as well as the effective load. This phenomenon will be discussed in detail in section 4.3.

As the concentration of α-ZrP nanoparticles is increased, the friction coefficient also increases, with the performance improvement dropping to 19% for the 0.25% concentration specimen.

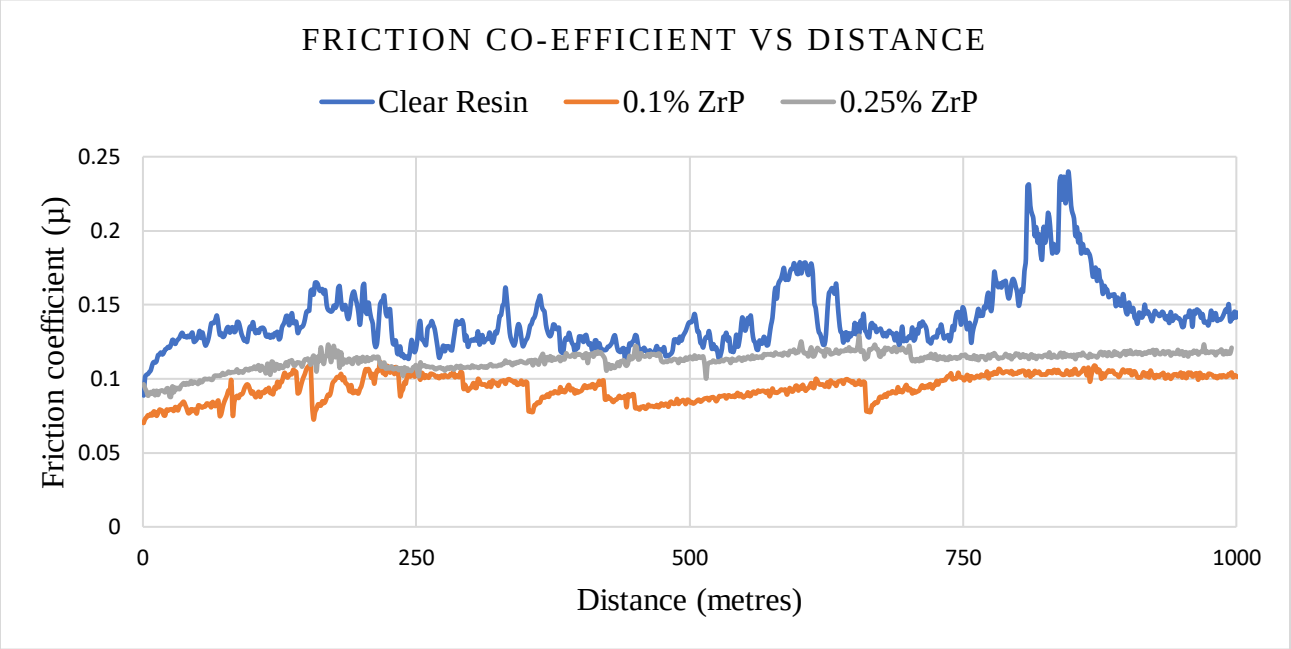

Figure 18. Friction performance of clear resin sample (without nanoparticles) and samples containing 0.1% and 0.25% α-ZrP nanoparticles by weight)

The friction test data is used to compute the average friction coefficient value for the different specimens. This data is shown in figure 19. The addition of α-ZrP NPs improves friction performance and reduces friction coefficient of the clear resin specimen from 0.14 to an impressive 0.095. These results show that tiny amounts of α-ZrP NPs (≤0.1wt %) can provide significant improvement in friction performance, and as such α-ZrP NPs are suitable additives for SLA printing applications and can be used to design and synthesize novel photopolymer nanocomposites with superior friction performance.

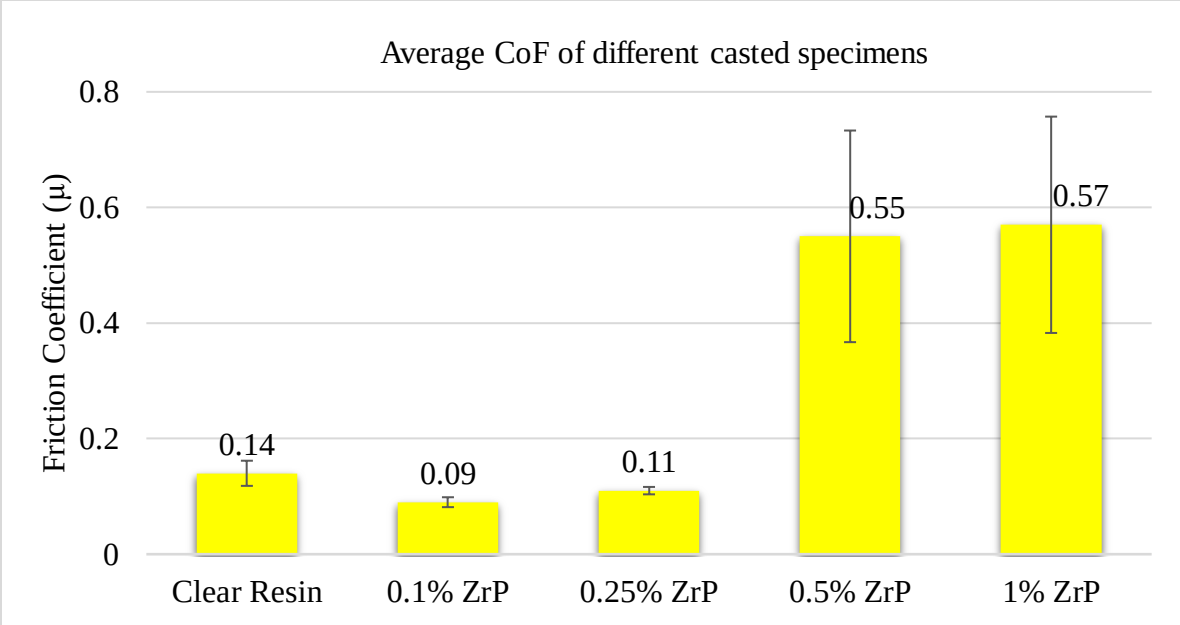

Figure 19. Average coefficient of friction for the different casted samples

4.1.2. Dispersion of α-ZrP in clear resin

Homogeneous dispersion of nanoparticles in the polymer matrix is critical for achieving optimal tribological performance. Optical microscopy is used to examine the dispersion of α-ZrP NPs in clear resin. Figure 20 shows the optical microscopic images of clear resin specimen (without nanoparticles) and nanocomposite containing 0.1% α-ZrP nanoparticles by weight. For the specimen with 0.1% nanoparticle concentration, homogeneous distribution of nanoparticles is observed.

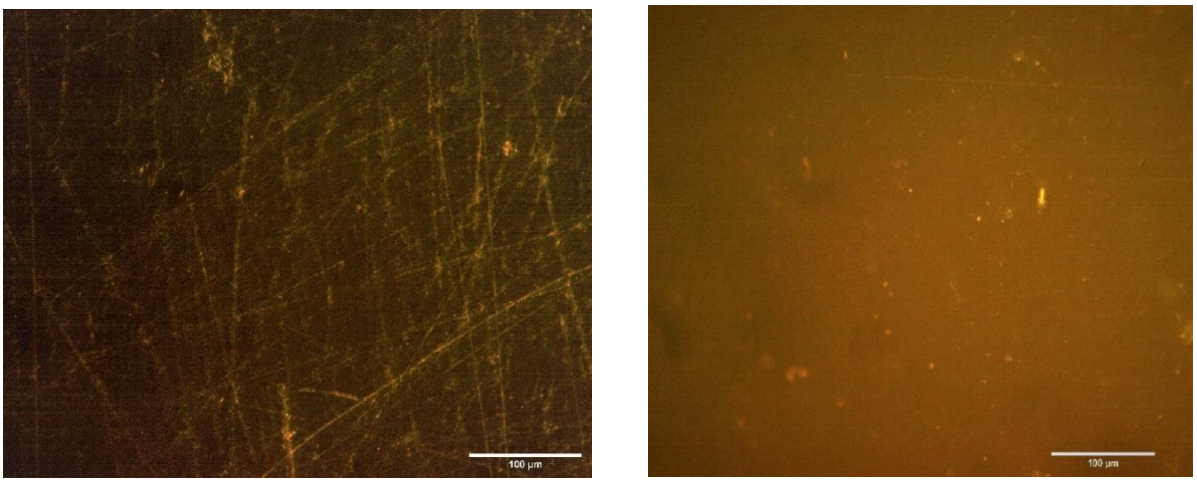

Figure 20. OM images of Clear Resin (left) and nanocomposite containing 0.1% α-ZrP at 20x.

Figure 21 shows the optical microscopic images of nanocomposites containing 0.25% (left) and 0.50% (right) α-ZrP nanoparticles by weight. Agglomeration of nanoparticles is observed as the concentration of α-ZrP nanoparticles increase. OM image of the 0.50% nanoparticle concentration specimen shows a significantly high number of nanoparticle agglomerates.

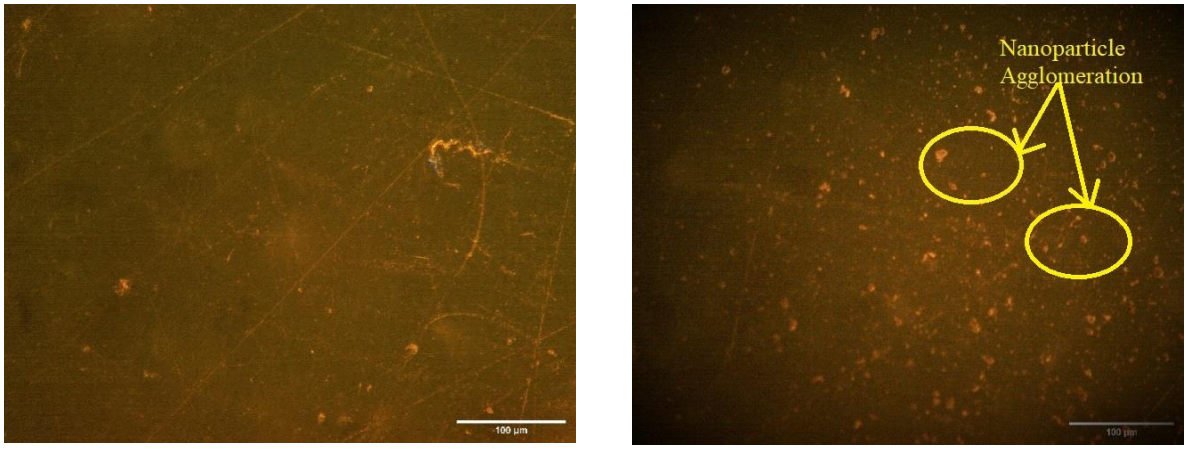

Figure 21. OM images of 0.25% (left) and 0.5% α-ZrP at 20x.

Agglomeration of particles leads to a reduction in surface free energy and a decrease in the surface area of the nanoparticles. Nanoparticle agglomerates are formed when particles adhere to each other by weak forces and form (sub)micron-sized entities[65]. Due to nanoparticle agglomeration, the friction performance of specimens deteriorate as the nanoparticle concentration increases.

These results indicate that optimal dispersion is achieved with a 0.1% nanoparticle concentration and this leads to a 32% improvement in friction performance (as compared to pure clear resin) with an impressive coefficient of friction value of 0.095.

4.1.3. Comparison with MoS_2

Molybdenum disulphide is a well-known anti-wear additive and is commonly used as a solid lubricant. MoS_2 nanoparticles have been shown to reduce friction and wear in metals[52-54] as well as in non-metallic coatings[55, 56]. In this study, we have compared the tribological performance of the best performing α-ZrP photopolymer nanocomposite (0.1 % wt.) with that of MoS_2 photopolymer nanocomposite containing the same concentration of MoS_2 nanoparticles. All fabrication parameters such as mixing time, curing time, post-curing processes have been kept the same for the both specimens.

Fig. 22 compares the friction performance of the best-performing α-ZrP specimen (0.1 % wt.) with that of a 0.1 % wt. MoS_2 specimen for a 1000 m reciprocating friction test using the pin-on-disc tribometer. It is observed that the 0.1 wt. % α-ZrP specimen maintains a stable friction coefficient varying between 0.09-0.10. However, for the MoS_2 specimen, the friction performance progressively degrades starting with a starting CoF value of ~0.14 and ending with a high CoF

value of ~0.63. From this result, it is evident that α-ZrP specimen performs significantly better than the MoS_2 specimen throughout the entire duration of the friction test.

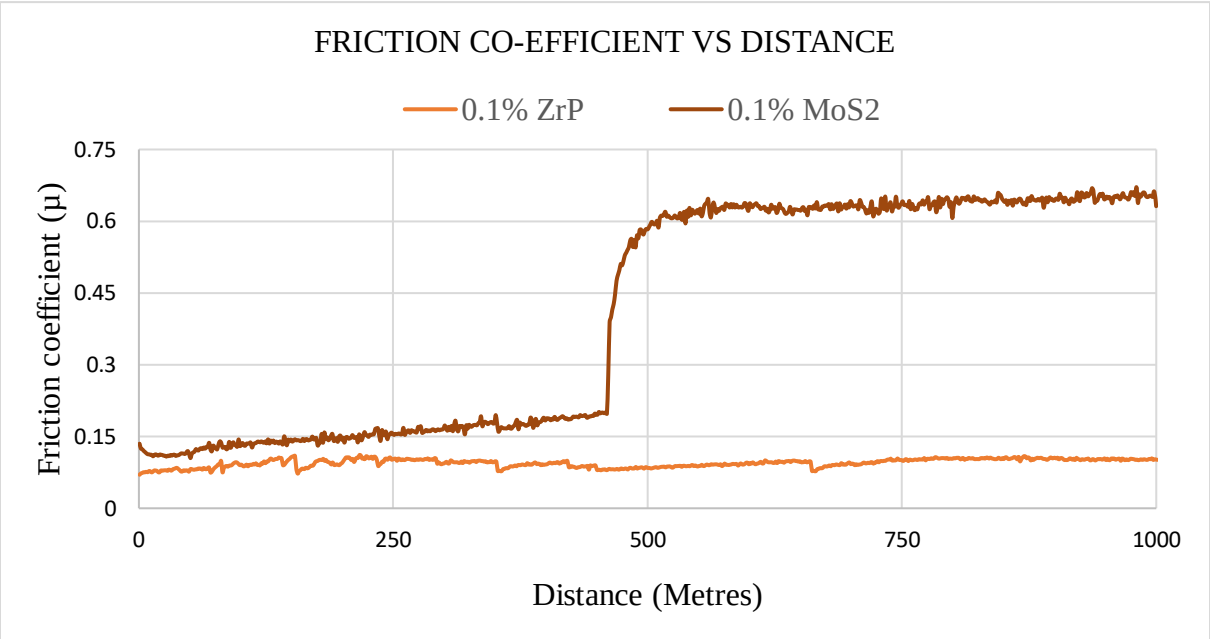

Figure 22. Friction performance of α-ZrP & MoS_2 (0.1 % wt.) specimens

Figure 23 shows the average CoF values for the α-ZrP and MoS_2 specimens calculated over the entire length of the friction test. It is observed that the MoS_2 specimen exhibits a CoF value that is ~350 times higher than that of the α-ZrP specimen.

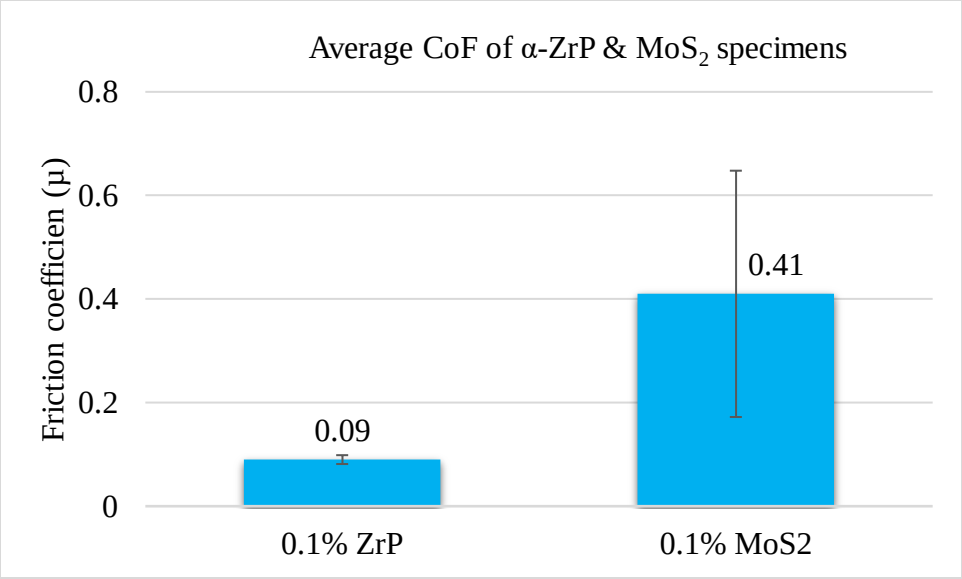

Figure 23. Average coefficient of friction for α-ZrP & MoS_2 (0.1 % wt.) specimens

Figure 24 shows the OM image of the MoS_2 taken at 20x magnification. It is observed that there is agglomeration of nanoparticles in the polymer matrix. This indicates that in the polymer matrix MoS_2 nanoparticles tend to adhere to each other, forming nanoparticle agglomerates with reduced surface area and reduced surface free energy.

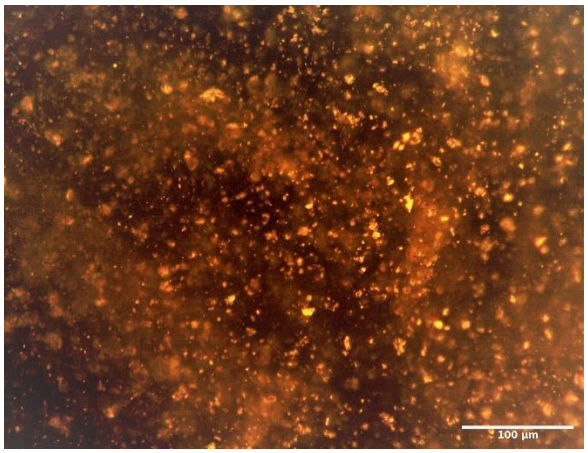

Figure 24. OM image of MoS_2 specimen

These results indicate that, with standard SLA clear resins and under low concentrations of nanoparticles, α-ZrP nanoparticles are superior to MoS_2 nanoparticles as anti-friction additives and can be used to achieve significant reduction in friction coefficient.

4.2. Wear Behavior

This section the wear behavior of the different casted specimens is discussed. It is observed that the low concentrations of α-ZrP nanoparticles (≤ 0.25 % wt.) in the polymer matrix significantly improves the wear resistance of clear resin. Five tribometer wear tests are conducted for each specimen to confirm repeatability of results.

In this section, we analyze the wear track of the worn surfaces, subjected to a 1000m wear test under 1N load on the pin-on-disc tribometer. Wear track morphology is characterized using optical microscopy. Wear volume is calculated using optical microscopic and interferometric data. Finally, the wear resistance of the best-performing α-ZrP photopolymer nanocomposite is compared with that of MoS_2 photopolymer nanocomposite, fabricated using the same parameters and containing identical concentration of MoS_2 nanoparticles.

4.2.1. Analysis of wear track

This section analyzes the wear track of the worn surfaces of the casted specimens. Fig. 25 shows the optical microscopic image of the wear track of the clear resin specimen taken at 5x and 10x magnifications. Figures 26, 27, 28 and 29 show the OM images of the wear tracks of the casted specimens, containing different weight percentages of α-ZrP nanoparticles, taken at 5x and 10x magnifications.

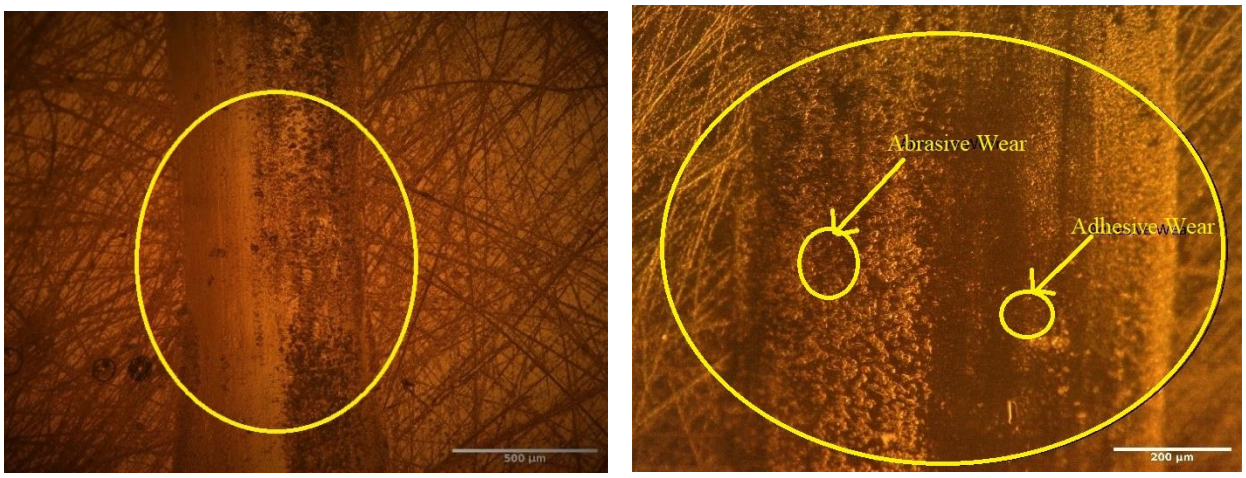

Figure 25. OM images of the wear track of clear resin specimen at 5x (left) and 10x (right) magnifications.

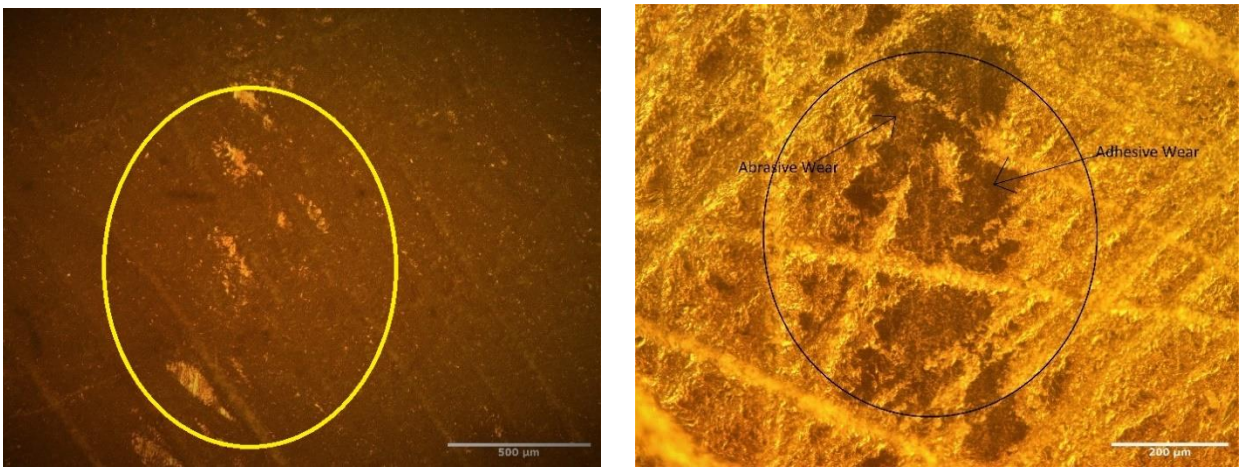

Figure 26. OM images of the wear track of 0.1 % wt. α-ZrP specimen at 5x (left) and 10x (right) magnifications.

In figures 25 and 26, the portions marked by the circles indicate the wear track on the worn surfaces of the specimens. It is observed that for the 0.1 % wt. α-ZrP specimen, the width of the wear track

is much narrower as compared to that of the clear resin specimen. This indicates that the addition of α-ZrP nanoparticles caused a reduction in the surface deformation thereby increasing the wear resistance of the specimen.

Both the specimens (clear resin and 0.1 % wt. α-ZrP) show a mix of adhesive and abrasive wear. It is observed that for the clear resin sample, adhesive wear is the more dominant form of wear, whereas for the 0.1 % wt. α-ZrP specimen, abrasive wear is more dominant. This is attributed to the low friction coefficient value and low adhesive bonding strength at the contact interface, achieved as a result of the addition of α-ZrP nanoparticles. The higher value of friction coefficient of the clear resin specimen, along with the higher adhesive bonding strength at the contact interface[66], leads to greater adhesive wear for the same.

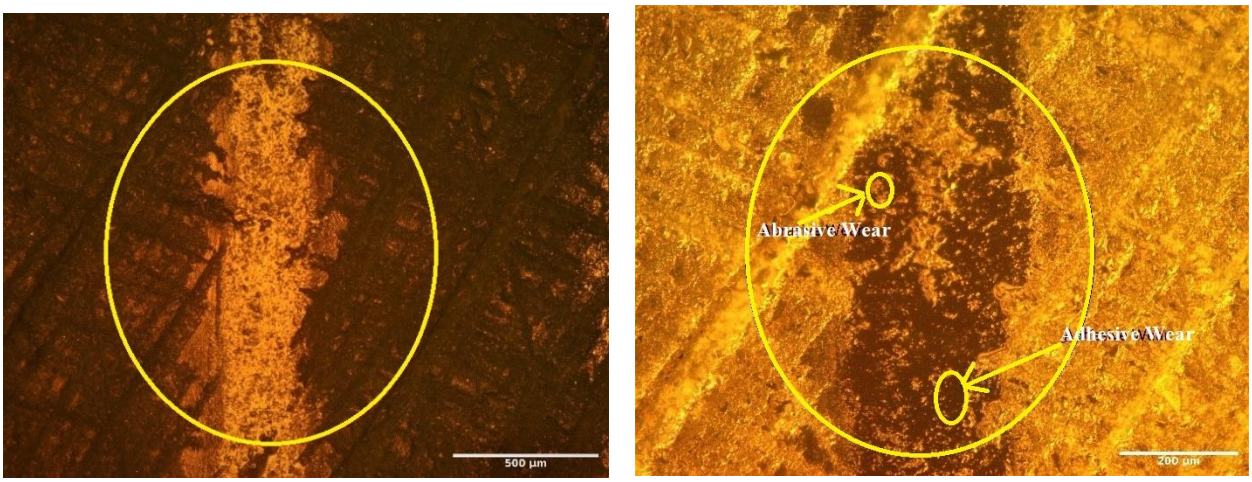

Figure 27. OM images of the wear track of 0.25 % wt. α-ZrP specimen at 5x (left) and 10x (right) magnifications.

Figure 27 shows the OM images of the wear track of the 0.25 % wt. α-ZrP specimen. Similar to the 0.1 % wt. α-ZrP specimen, this specimen also shows a narrower wear track as compared to the clear resin specimen. The wear track shows both adhesive and abrasive forms of wear. From the 10x magnification OM image it is observed that abrasive wear is the more dominant form of wear for this specimen. This is because of the lower value of friction coefficient and lower adhesive bonding strength at the contact interface for this specimen.

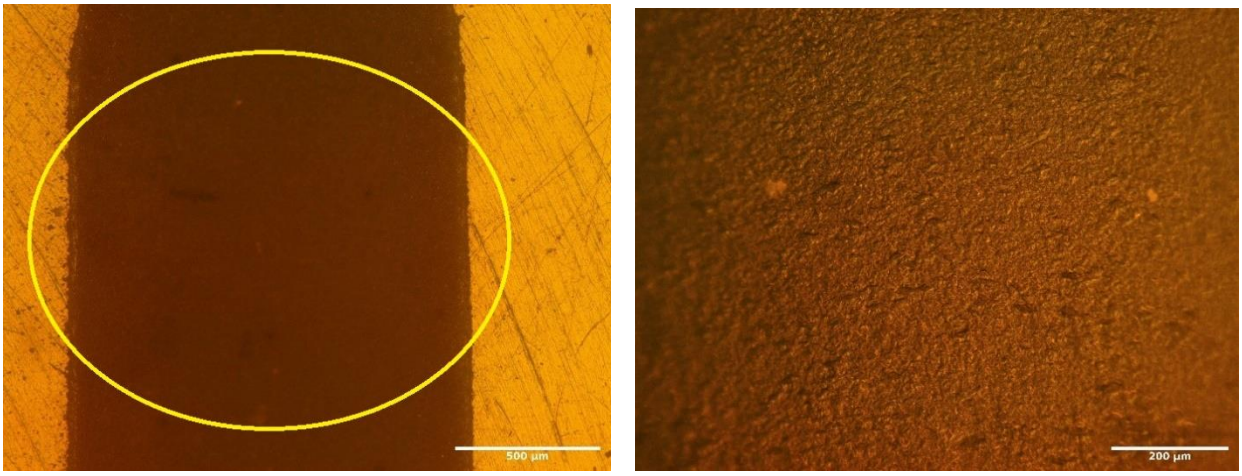

Figure 28. OM images of the wear track of 0.5 % wt. α-ZrP specimen at 5x (left) and 10x (right) magnifications

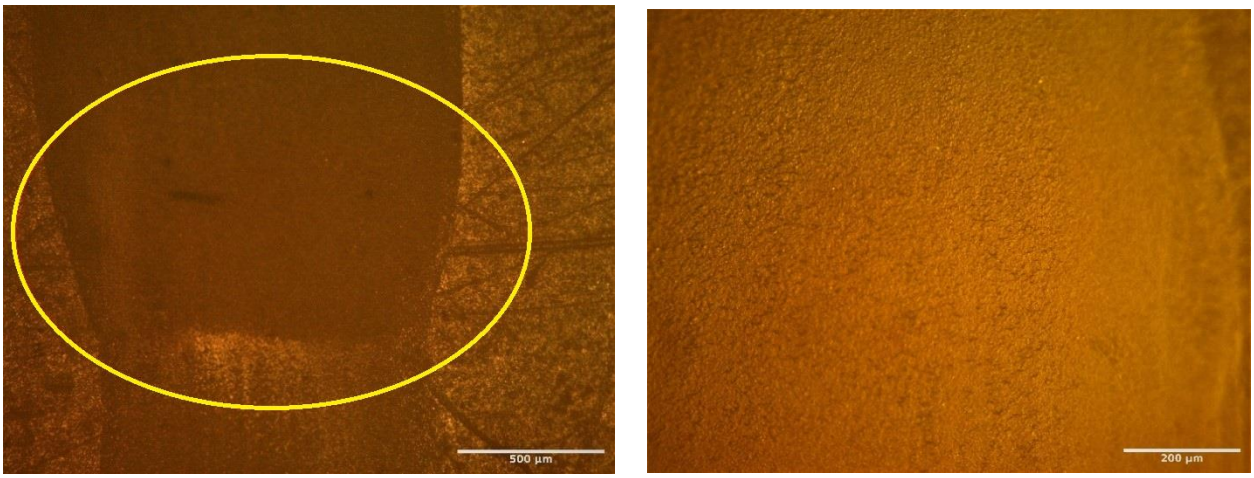

Figure 29. OM images of the wear track of 1 % wt. α-ZrP specimen at 5x (left) and 10x (right) magnifications.

Figures 28 and 29 shows the OM images of the wear tracks of the 0.5 % wt. and 1 % wt. α-ZrP specimens. For these two specimens, the width of the wear track is wider as compared to the clear resin specimen. Moreover, the 10x magnification OM images indicate that these specimens exhibit mostly adhesive wear with very little or no abrasive wear. This can be attributed to the significantly high value of friction coefficient and high adhesive bonding strength at the contact interface, exhibit by both of these specimens.

OM imaging data has been used to calculate the wear track width for the different casted specimens. This data is provided in table 7. Width values have been measured at 5 different points on the wear track and using this data an average wear track width has been calculated for each specimen.

Table 7. Comparison of wear track width of different casted specimens

No.	Clear Resin (µm)	0.1 % wt. α-ZrP (µm)	0.25% wt. α-ZrP (µm)	0.5 % wt. α-ZrP (µm)	1 % wt. α-ZrP (µm)
1	631.3	245.3	327.1	1361.6	1125
2	648.9	152.9	379.1	1370	1384.3
3	616.5	191.2	375.6	1279.8	1448.7
4	696.1	218.7	356.3	1321.2	1453.7
5	730.4	292.8	306.3	1288.7	1351.4
Average	664.6	220.2	348.9	1324.2	1352.6
Standard Deviation	±42	±45	±28	±36	±120

As seen from table 7, the 0.1 % wt. and 0.25 % wt. α-ZrP specimens show a 66% and 47% decrease in average wear track width as compared to the clear resin specimen. These results clearly indicate that low concentrations of α-ZrP nanoparticles (≤ 0.25 % wt.) are effective in significantly reducing wear track width of casted clear resin photopolymer nanocomposite specimens.

4.2.2. Evaluation of Wear volume and wear rate

As mentioned in section 4.2.1, OM imaging data is used to evaluate the average wear track width for the different casted samples. Interferometric data is used to evaluate the average wear track depth for each specimen. Figures 30, 31 and 32 show the interferometer results of the different casted samples with 2D and 3D analysis images.

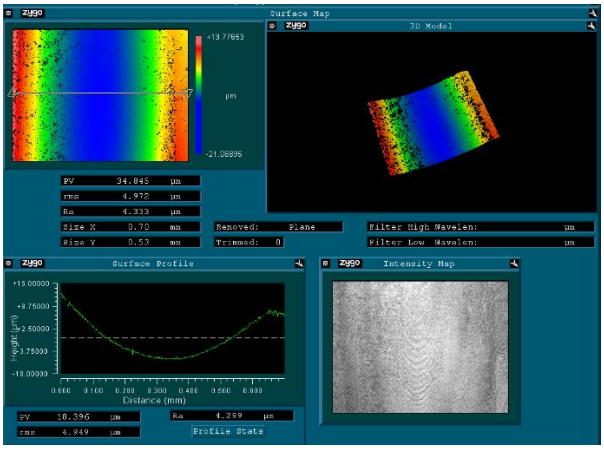

Figure 30. Interferometer results of clear resin specimen

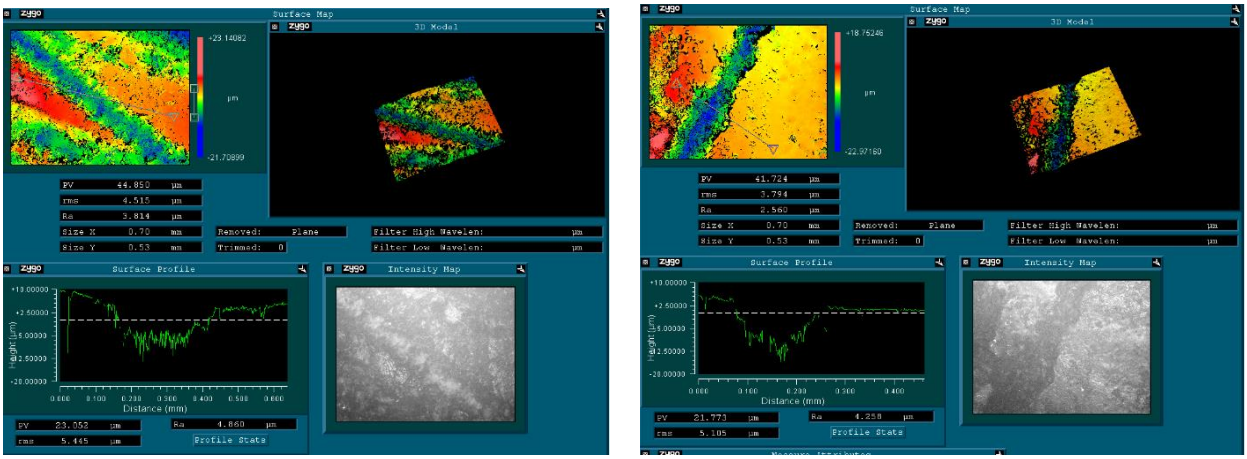

Figure 31. Interferometer results of 0.1 % wt. (left) and 0.25 % wt. (right) α-ZrP specimens

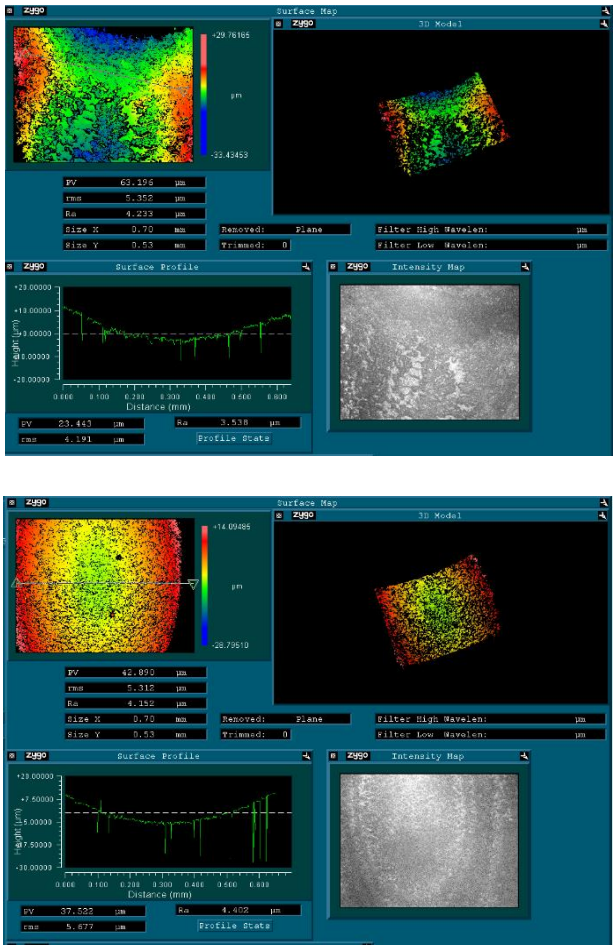

Figure 32. Interferometer results of 0.5 % wt. (left) and 1 % wt. (right) α-ZrP specimens

Table 8 contains the depth values of the wear tracks for the different casted samples. Depth values have been measured at 5 different locations on the wear track and using this data an average value of wear depth has been calculated.

Table 8. Comparison of wear track depth of different casted specimens

No.	Clear Resin (μm)	0.1 % wt. α-ZrP (μm)	0.25% wt. α-ZrP (μm)	0.5 % wt. α-ZrP (μm)	1 % wt. α-ZrP (μm)
1	17.5	16	14.5	17	17.5
2	16	17	15.5	13	14.5
3	15.5	16.5	17.5	16.5	15
4	16.5	15	17	16	16
5	15.5	15	16	16.5	16
Average	16.2	15.9	15.8	15.8	15.8
Standard Deviation	±0.75	±0.8	±1.0	±1.4	±1.1

The results indicate that there is slight decrease (~ 2.5%) in the wear track depth with the addition of α-ZrP nanoparticles. This indicates that, unlike wear track width, the addition of α-ZrP nanoparticles does not impact the depth of the wear track to a significant extent and maintains the value nearly constant even with changing concentrations of the nanoparticles.

As mentioned in Chapter III, the wear volume is calculated as a product of the wear track width, wear track depth and wear track length (or sliding distance for the wear test). Wear rate is calculated using the wear volume, sliding distance and applied load. Table 9 contains the wear volume and wear rate for the different casted specimens.

Table 9. Wear volume and wear rate of different casted specimens

	Clear Resin	0.1 % wt. α-ZrP	0.25% wt. α-ZrP	0.5 % wt. α-ZrP	1 % wt. α-ZrP
Wear Volume (μm^3)	53832600	17505900	27563100	104611800	106855400
Standard Deviation (μm^3)	±157500	±180000	±140000	±252000	±660000
Wear Rate (μm^3/N- μm)	10766.52	3501.18	5512.62	20922.36	21371.08
Standard Deviation (μm^3/N- μm))	±31.4	±36	±28	±50.4	±132

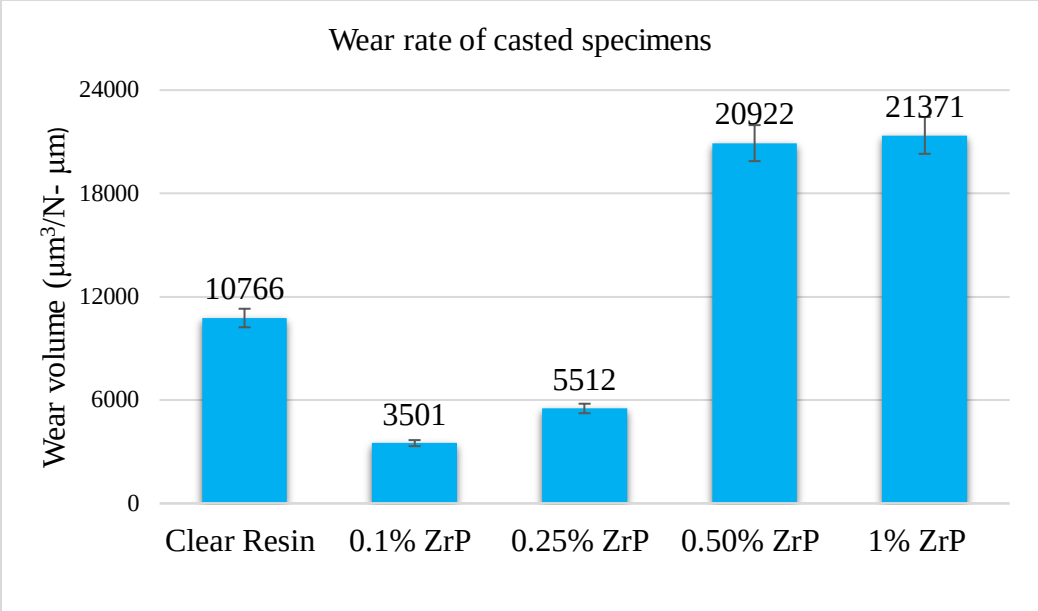

Figure 33. Comparison of wear rate of different casted specimens

Figure 33 compares the wear rate of the different casted specimens. The 0.1 % wt. α-ZrP specimen exhibits a 67% improvement in wear resistance whereas the 0.25 % wt. α-ZrP specimen exhibits a 48% improvement in wear resistance. These results indicate that the low concentrations (≤ 0.25 % wt.) of α-ZrP nanoparticles provide a significant improvement in the wear resistance of clear resin. The NPs shape and the layered structure of the α-ZrP nanoparticles combine together to provide this improvement in wear resistance. The disc-shaped nanoparticles enter into the spatial region between the mating surfaces and effectively carry a load, thereby decresaing the effective contact area of the mating surfaces as well as the effective load. Alongside, the double-layered structure of the α-ZrP nanoparticles, and the weak Van der Waals forces between the discs, aide this process and lower the shear stress at the contact surface. Moreover, the weak links between the discs of the α-ZrP nanoparticles cause the exfoliated layers to be smaller than the asperity

heights, causing the asperities to act as reservoirs, covering the surface[66]. This phenomenon will be discussed in detail in section 4.3.

4.2.3. Comparison with MoS_2

In this section, we conduct a wear analysis of the photopolymer nanocomposite containing 0.1% MoS_2 by weight. The fabrication parameters for this specimen are kept the same as for all the other casted specimens. Wear track morphology is characterized using optical microscopy. Wear volume and wear rate is calculated using optical microscopic and interferometric data. Finally, the results are compared with those of the 0.1 % wt. α-ZrP specimen.

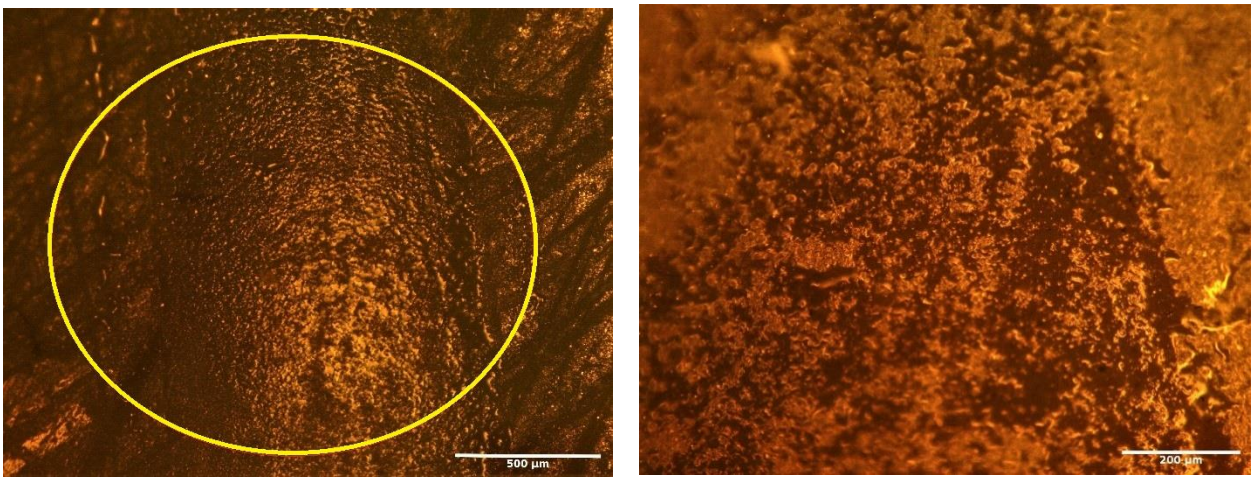

Figure 34. OM images of the wear track of 0.1 % wt. MoS2 specimen at 5x (left) and 10x (right) magnifications.

Figure 34 shows the OM images of the wear track of the 0.1 % wt. MoS_2 specimen. It is observed that the wear track is much wider than that for the 0.1 % wt. α-ZrP specimen. This indicates a higher rate of surface deformation for this specimen as compared to the 0.1 % wt. α-ZrP specimen. From the 10x magnified OM image it is observed that the wear track shows both adhesive and

abrasive forms of wear, with the former being more dominant. This is due to the high friction coefficient value and high adhesive bonding strength at the contact interface, for this specimen.

OM imaging data has been used to compute the wear track width for the 0.1 % wt. MoS_2 specimen. This data is provided in table 10. Width values have been measured at 5 different points on the wear track and using this data an average wear track width has been calculated.

Table 10. Wear track width of 0.1 % wt. MoS_2 specimen

No.	1 (µm)	2 (µm)	3 (µm)	4 (µm)	5 (µm)	Average (µm)	Standard Deviation (µm)
0.1 wt% MoS_2	1135.4	1287.2	1229.6	1301.3	1201.3	1230.9	±67.3

These results clearly show that the wear track width is significantly higher for the 0.1 % wt. MoS_2 specimen as compared to the 0.1 % wt. α-ZrP specimen. This indicates that at low concentrations, α-ZrP nanoparticles are much more effective as compared to MoS_2 nanoparticles, in reducing surface deformation and wear track width of casted clear resin photopolymer nanocomposite specimens.

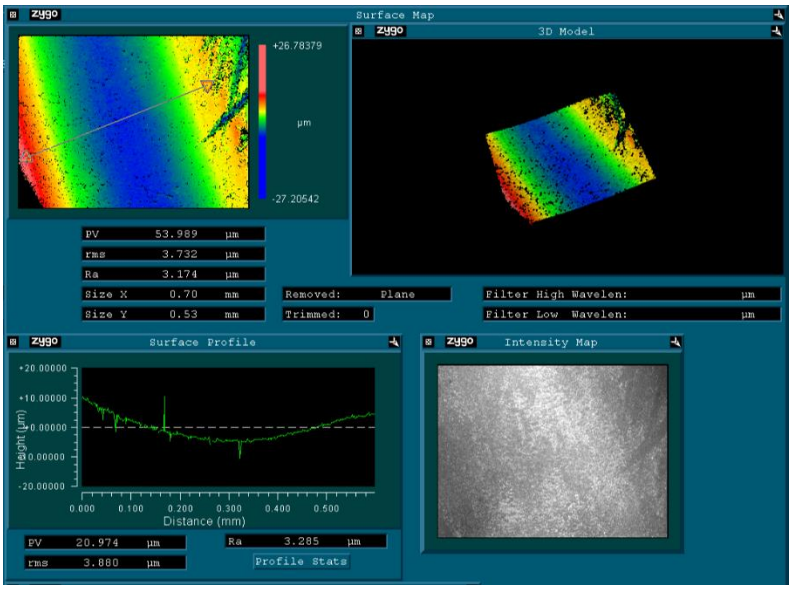

Figure 35. Interferometer results of 0.1 % wt. MoS_2 specimen

Interferometric data is used to calculate the average wear depth for the MoS_2 specimen. Figure 35 shows the interferometer results of the 0.1 % wt. casted MoS_2 specimen samples with 2D and 3D analysis images. Table 11 contains the depth values of the wear track for the specimen. Depth values have been measured at 5 different locations on the wear track and using this data an average value of wear depth has been calculated.

Table 11. Wear track depth of 0.1 % wt. MoS_2 specimen

No.	1 (µm)	2 (µm)	3 (µm)	4 (µm)	5 (µm)	Average (µm)	Standard Deviation (µm)
0.1 wt% MoS_2	17.5	14.5	15.5	15	16.5	15.8	±1.2

The results indicate that there is very slight decrease (< 1 %) in the wear track depth of the 0.1 % wt. MoS_2 specimen as compared to the 0.1 % wt. α-ZrP specimen. Comparing this with the results obtained in section 4.2.2, this indicates that the addition of nanoparticles has negligible impact on the wear track depth of clear resin.

Table 12 contains the wear volume and wear rate for the 0.1 % wt. MoS_2 specimen. This data is calculated using the average wear track width, depth & length values, along with the sliding distance and applied load (for wear volume).

Table 12. Wear volume and wear rate of 0.1 % wt. MoS_2 specimen

	Value	Standard Deviation
Wear Volume (μm^3)	97241100	±403800
Wear Rate (μm^3/N- μm)	19448	±80.7

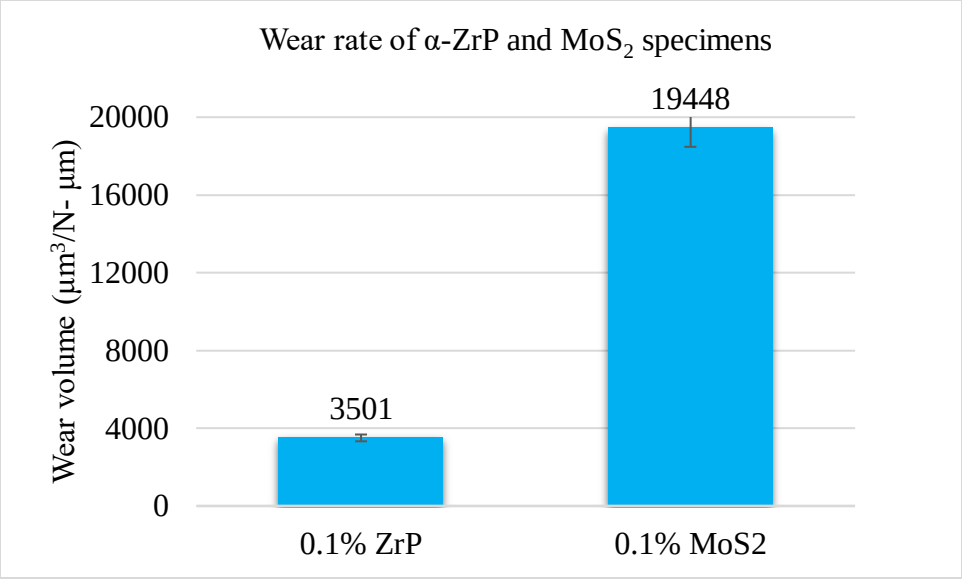

Figure 36. Comparison of wear rate of ZrP and MoS_2 casted specimens

Figure 36 compares the wear rate of the 0.1 % wt. α-ZrP and 0.1 % wt. MoS_2 specimens. The α-ZrP specimen exhibits significantly better wear resistance as compared to the MoS_2 specimen.

These results indicate that, with standard SLA clear resins and under low concentrations of nanoparticles, α-ZrP nanoparticles are superior to MoS_2 nanoparticles as anti-wear additives and can be used to achieve significant reduction in wear.

4.3. Mechanisms of α-ZrP NPs on tribological performance of casted samples

The experimental results discussed in section 4.1 and 4.2 clearly indicate that low concentrations of α-ZrP (≤ 0.25 % wt.) significantly reduced friction and wear of casted clear resin samples. This phenomenon has been explained below using two different mechanisms.

The disc-like shape of the α-ZrP nanoplatelets, are an important factor in enhancing the friction and wear performance of the nanocomposites. The disc-like shape of the nanoplatelets allows them to enter into the contact region between the mating surfaces. These nanoplatelets carry a load on their surfaces thereby decreasing the effective load and contact-area of the mating surfaces. By effectively reducing the contact area of asperities on the mating surfaces, the NPs reduce cold welding of asperities and lower the amount of adhesive wear. This also lowers the shear stress, which leads to decresed friction between the contact surfaces.

The layered structure of α-ZrP nanoplatelets is also an important factor in enhancing the tribological properties. In α-ZrP nanoplatelets, the layered structure is formed by the zirconium atoms connecting to the phosphate groups via oxygen atoms. As shown is figure 37, using hydrogen bonds, the layer is bonded parallel to its adjacent layer while maintaining a space of 7.6 Å[67]. Under a shearing force, the hydrogen bonds, which are relatively weak, allow the adjacent layers to be easily exfoliated. This leads to easier and more efficient dispersion of wear energy. The valleys of asperities easily trap these exfoliated layers leading to the formation of physical barriers[68]. α-ZrP nanoplatelets can get accumulated in the contact area between asperities of the mating surfaces. This modifies the shear line and leads to an artificial smoothening out of the surface.

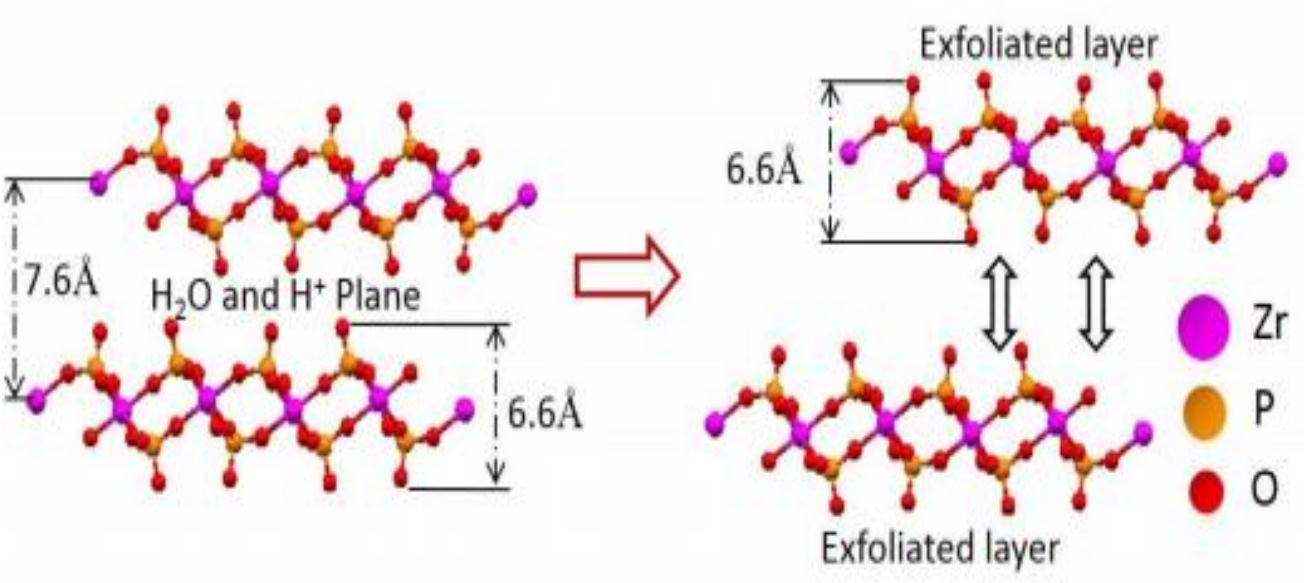

Figure 37. Exfoliated layers of α-ZrP. Reprinted with permission from [67].

In the present research, casted samples containing disc-like nanoparticles of α-ZrP were examined. Based on the observation through optical microscope shown in Figs. 4.4 and 4.5 the particles were distributed with visible agglomeration when the concentration is increased (Fig. 38). The particles that appear on the surface are those affecting the friction. The aggregated particles are believed to sustain shear force due to interparticle interactions. This is the reason why friction increases with increased concentration (Fig. 17, 19, 21).

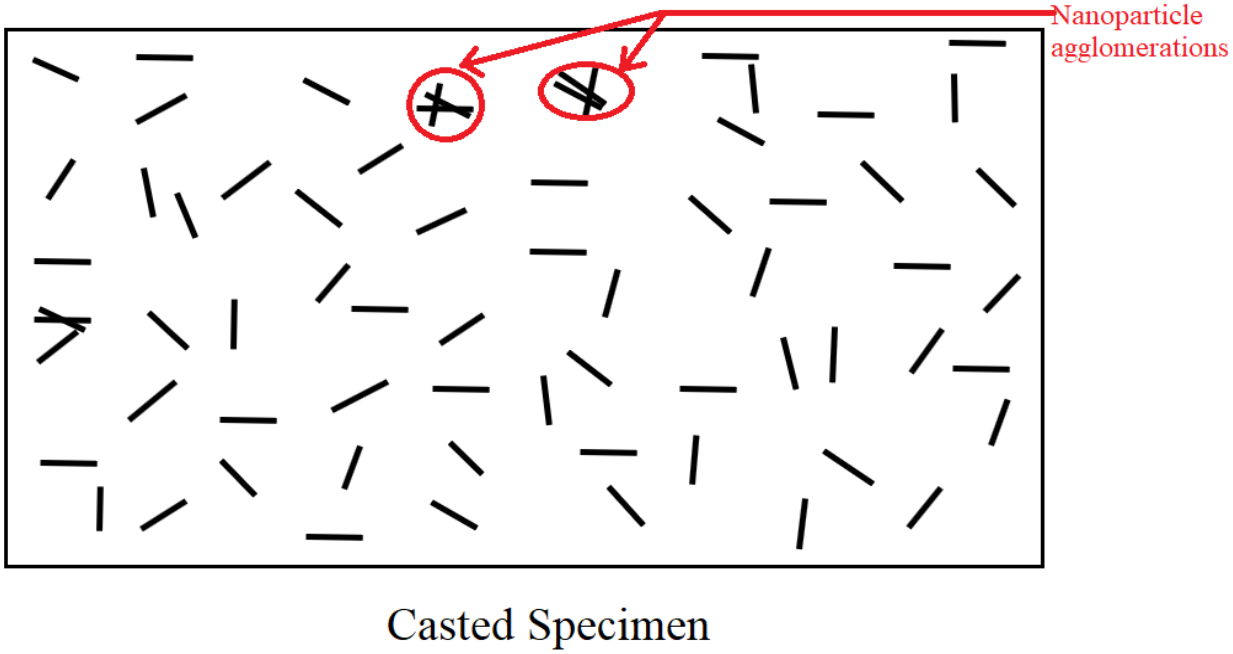

Figure 38. Distribution α-ZrP nanoplatelets in casted specimen

Thus, under low concentrations of α-ZrP nanoparticles (≤ 0.25 % wt.), a notable improvement in wear (19-32%) and friction (48-65%) performance is observed. But as the concentration is increased, increased agglomerations lead to a deterioration in performance. Under 0.1 % wt. concentration of α-ZrP nanoparticles, optimal friction and wear performances are observed.

CHAPTER V

TRIBOLOGICAL EVALUATION OF 3D PRINTED PHOTOPOLYMER NANOCOMPOSITES

This chapter discusses the influence of α-ZrP nanoparticles on the tribological performance of 3D printed clear resin & nanocomposite samples. In the first section, the effects of 0.1 % wt. of α-ZrP NPs on the friction performance of 3D printed clear resin nanocomposites is discussed. This concentration of α-ZrP NPs is selected based on the results obtained from the tribological performance of the different casted nanocomposite specimens discussed in Chapter IV.

In the second section, the effects of 0.1 % wt. of α-ZrP nanoparticles on the wear performance of 3D printed clear resin nanocomposites is analyzed. Wear performance is examined with respect to wear morphology and wear rate. Finally, the effect of nanoparticle shape and morphology on the wear mechanism of α-ZrP photopolymer nanocomposite is examined in detail.

5.1. Frictional Behavior

In the section, we analyze the friction performances of 3D printed clear resin and 3D printed 0.1 % wt. α-ZrP clear resin nanocomposite specimens. The specimens are subjected to 1000m reciprocating friction test using the pin-on-disc tribometer at room temperature. Friction data captured using the TriboX software is used to generate graphs, showing the variation of friction

coefficient with distance. Five such tribometer friction tests are conducted for each specimen to confirm repeatability of results.

5.1.1. Comparison of friction performance

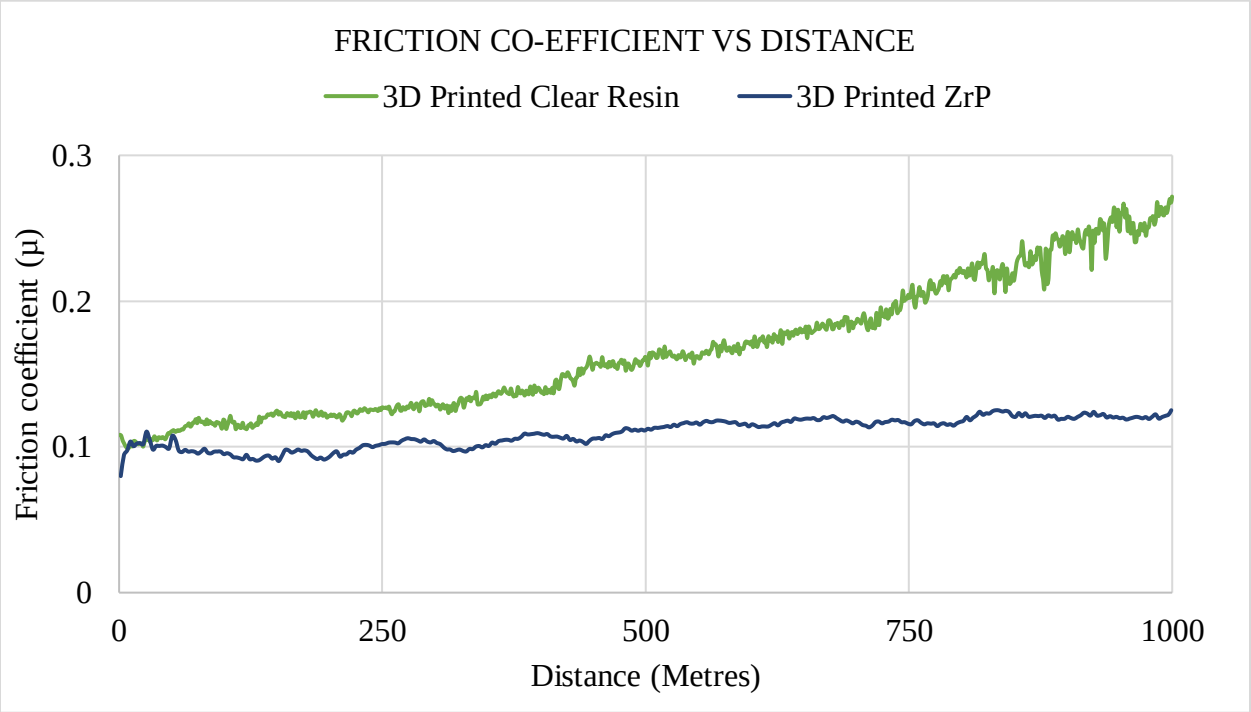

Figure 39. Friction behavior of 3D printed clear resin and 0.1 % wt. α-ZrP clear resin nanocomposite specimens

Figure 39 shows the friction behavior of the two 3D printed specimens. The results indicate a considerable reduction in friction coefficient for the 0.1 % wt. α-ZrP clear resin nanocomposite specimen. It is also observed that, for the 3D printed clear resin specimen the friction coefficient increases progressively with distance, whereas the 3D printed α-ZrP clear resin nanocomposite specimen maintains a stable friction coefficient throughout the entire duration of the friction test. The considerable reduction in friction coefficient for the nanocomposite can be explained by the

improved alignment of α-ZrP within each layer of the 3D printed specimens This along with the disc-like shape of nanoparticles lead to lower shear stress and lower friction for the 3D printed specimen.

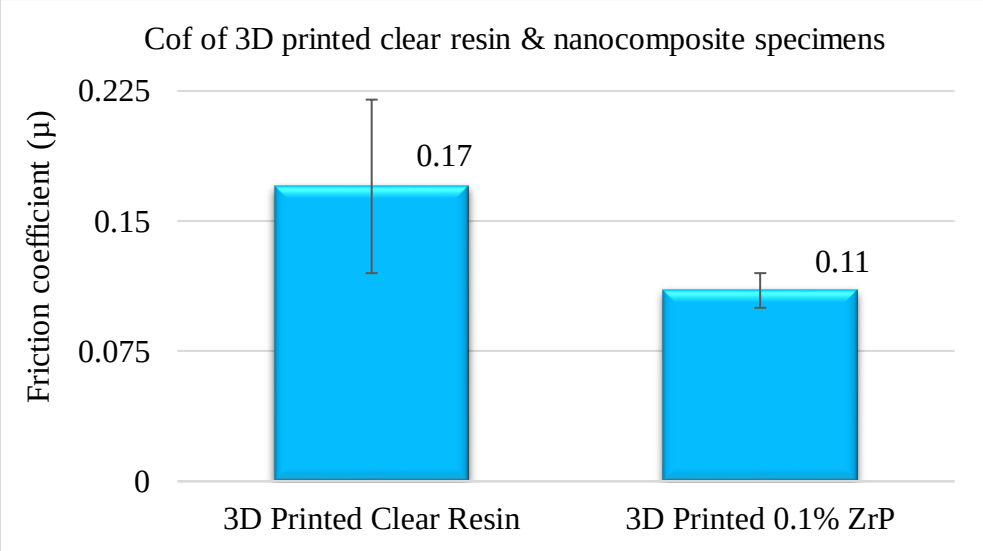

Figure 40. Average coefficient of friction for 3D printed clear resin and 3D printed nanocomposite specimens

The friction test data is used to compute the average friction coefficient value for the 3D printed specimens. This data is shown in figure 40. The addition of α-ZrP NPs improves friction performance and reduces friction coefficient from 0.17 to 0.11. This indicates an impressive 34% improvement in friction performance for the 3D printed nanocomposite specimen. These results indicate that tiny amounts of α-ZrP NPs (≤0.1wt %) can provide significant improvement in friction performance, and as such α-ZrP NPs are acceptable as additives for SLA printing applications and can be used to design and synthesize novel photopolymer nanocomposites with superior friction performance.

5.1.2. Dispersion of nanoparticles

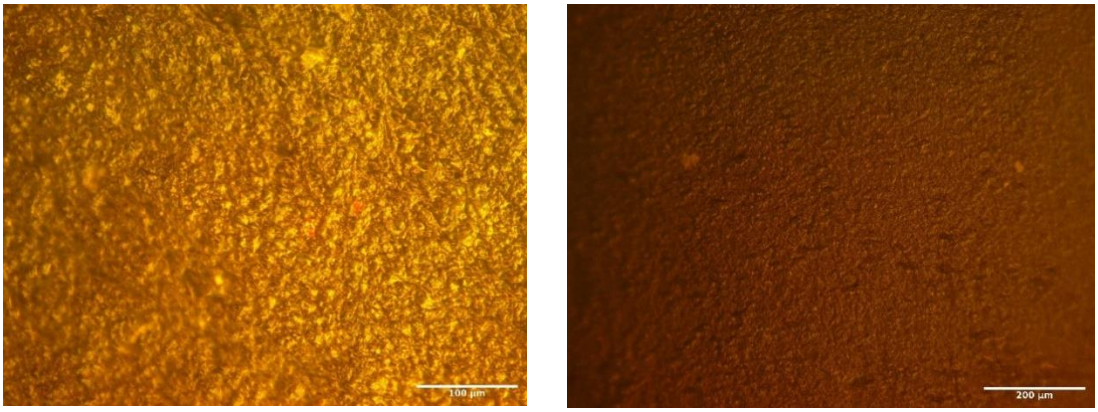

Figure 41. OM images of 3D printed clear resin (left) and nanocomposite (right) specimens

Optical microscopy is used to examine the dispersion of α-ZrP nanoplatelets in the clear resin matrix. Figure 41 shows the optical microscopic images of 3D printed clear resin and 3D printed nanocomposite specimens. For the 3D printed 0.1 % wt. α-ZrP clear resin nanocomposite specimen, homogeneous distribution of nanoparticles is observed. Homogeneous dispersion of nanoparticles in the polymer matrix is critical for achieving optimal tribological performance.

5.2. Wear Behavior

This section discusses the wear behavior of the 3D printed specimens. It is observed that the 0.1 % wt. α-ZrP clear resin nanocomposite specimen exhibits significantly improved wear resistance as compared to the 3D printed clear resin specimen. Five tribometer wear tests are conducted for each specimen to confirm repeatability of results.

In this section, we examine the wear track for the different specimens, generated from a 1000m wear test under 1N load on the pin-on-disc tribometer. Wear track morphology is characterized

using optical microscopy. Wear volume is calculated using optical microscopic and interferometric data.

5.2.1. Analysis of wear track

This section analyzes the wear track of the worn surfaces of the 3D printed specimens. Figures 42 and 5.5 show the optical microscopic image of the wear track of the 3D printed clear resin and α-ZrP clear resin nanocomposite specimens taken at 5x and 10x magnifications.

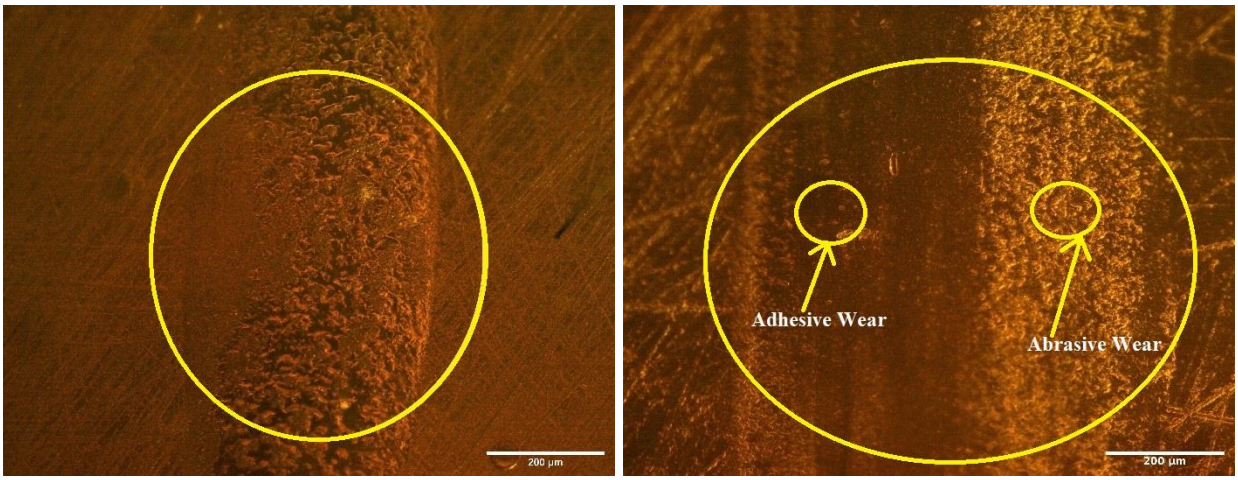

Figure 42. OM images of the wear track of 3D printed clear resin specimen at 5x (left) and 10x (right) magnifications.

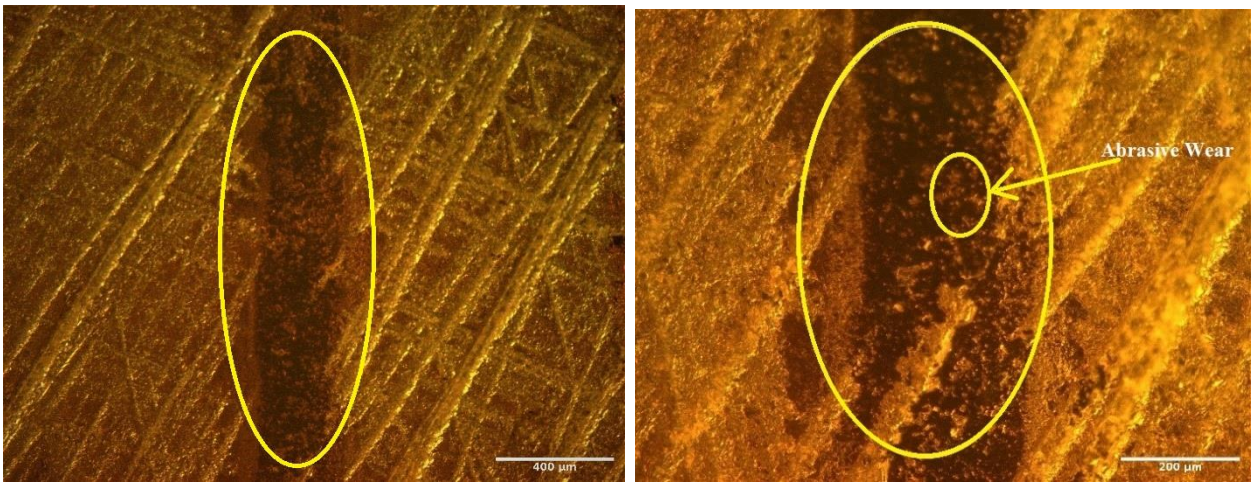

Figure 43. OM images of the wear track of 3D nanocomposite specimen at 5x (left) and 10x (right) magnifications.

In figure 42 and 43, the portions marked by the circles indicate the wear track on the worn surfaces of the 3D printed specimens. It is observed that for the 0.1 % wt. α-ZrP nanocomposite, the width of the wear track is significantly narrower as compared to that of the clear resin specimen. This indicates that the addition of α-ZrP nanoparticles caused a reduction in the surface deformation thereby increasing the wear resistance of the specimen.

Both the specimens show a mix of adhesive and abrasive wear. It is observed that for the clear resin specimen, adhesive wear is the more dominant form of wear, whereas for the nanocomposite specimen, abrasive wear is more dominant. This is attributed to the low friction coefficient value and low adhesive bonding strength at the contact interface, achieved as a result of the addition of α-ZrP nanoparticles. The higher value of friction coefficient of the clear resin specimen, along with the higher adhesive bonding strength at the contact interface[66], leads to greater adhesive wear for the same.

OM imaging data has been used to evaluate the wear track width for the 3D printed specimens. This data is provided in table 13. Width values have been measured at 5 different points on the wear track and using this data an average wear track width has been calculated for each specimen.

Table 13. Wear track width of 3D printed specimens

No.	1 (µm)	2 (µm)	3 (µm)	4 (µm)	5 (µm)	Average (µm)	Standard Deviation
Clear Resin	426.3	491.5	471.9	501.3	450.2	468.2	±27.3
0.1 % wt. α-ZrP nanocomposite	171.5	152.97	191.2	166.6	141	164.6	±17

As seen from table 13, the 3D printed nanocomposite specimen exhibits a 64% reduction in wear track width as compared to the 3D printed clear resin specimen. These results indicate that α-ZrP nanoparticles are effective in significantly reducing wear track width of 3D printed nanocomposites.

5.2.2. Evaluation of wear volume and wear rate

As mentioned in section 5.2.1, OM imaging data is used to compute the average wear track width for the 3D printed specimens. Interferometric data is used to compute the average wear track depth for the specimens. Figure 44 shows the interferometer results of the 3D printed samples with 2D and 3D analysis images.

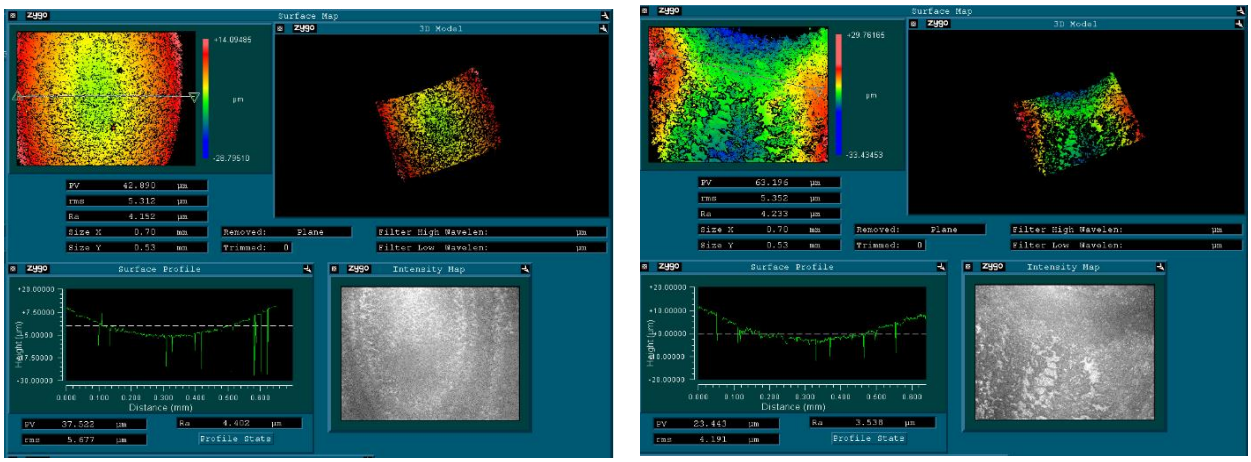

Figure 44. Interferometer results of 3D printed clear resin (left) and 0.1 % wt. α-ZrP clear resin nanocomposite specimens

Table 14 contains the depth values of the wear tracks for the 3D printed samples. Depth values have been measured at 5 different locations on the wear track and using this data an average value of wear depth has been calculated.

Table 14. Wear track depth of 3D printed specimens

No.	1 (µm)	2 (µm)	3 (µm)	4 (µm)	5 (µm)	Average (µm)	Standard Deviation
Clear Resin	11	14	12.5	11	13.5	12.4	±1.24
0.1 % wt. α-ZrP nanocomposite	10.5	11.5	14	12.5	12.5	12.2	±1.16

The results indicate that there is a slight decrease (~ 1.6%) in the wear track depth with the addition of α-ZrP nanoparticles. This indicates that, unlike wear track width, the addition of α-ZrP nanoparticles does not significantly impact wear track depth.

As mentioned in Chapter III, the wear volume is calculated as a product of the wear track width, wear track depth and wear track length (or sliding distance for the wear test). Wear rate is calculated using the wear volume, sliding distance and applied load. Table 15 contains the wear volume and wear rate for the different casted specimens.

Table 15. Wear volume and wear rate of different casted specimens

	Wear Volume (μm^3)	Standard Deviation	Wear Rate (μm^3/N- μm)	Standard Deviation
Clear Resin	29028400	169260	5805.68	±33.8
0.1 % wt. α-ZrP nanocomposite	10040600	98600	2008.12	±19.7

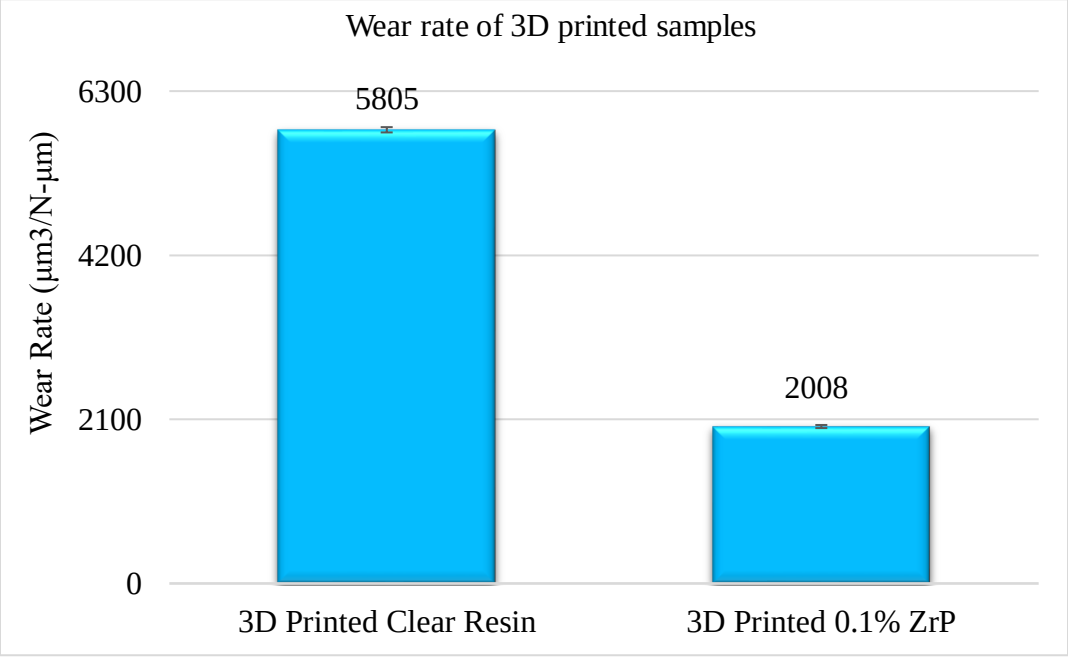

Figure 45. Comparison of wear rate of 3D printed samples

Figure 45 compares the wear rate of the 3D printed specimens. The 3D printed 0.1 % wt. α-ZrP nanocomposite specimen exhibits a 65% improvement in wear resistance as compared to the 3D printed clear resin specimen. These results indicate that the addition of low concentrations of α-ZrP nanoparticles can provide a significant improvement in the wear resistance of 3D printed parts. The layer-by-layer printing process, disc-like shape and layered structure of the α-ZrP nanoparticles combine together to provide this improvement in wear resistance. The disc-like shape of the α-ZrP nanoparticles allows the surface NPs to carry a load which in turn reduces the effective load acting on the surface. Alongside, the weak links in between the discs allow for easier exfoliation of the α-ZrP nanoparticles and lead to efficient dispersion of wear energy. The exfoliated layers are smaller than the heights of the asperities, causing the asperities to act as reservoirs which cover the surface[66]. This phenomenon will be discussed in detail in section 5.3.

These results imply that α-ZrP nanoparticles are acceptable as anti-friction and anti-wear additives for SLA printing applications and can be used (in low concentrations) to design and synthesize novel photopolymer nanocomposites with superior tribological performance.

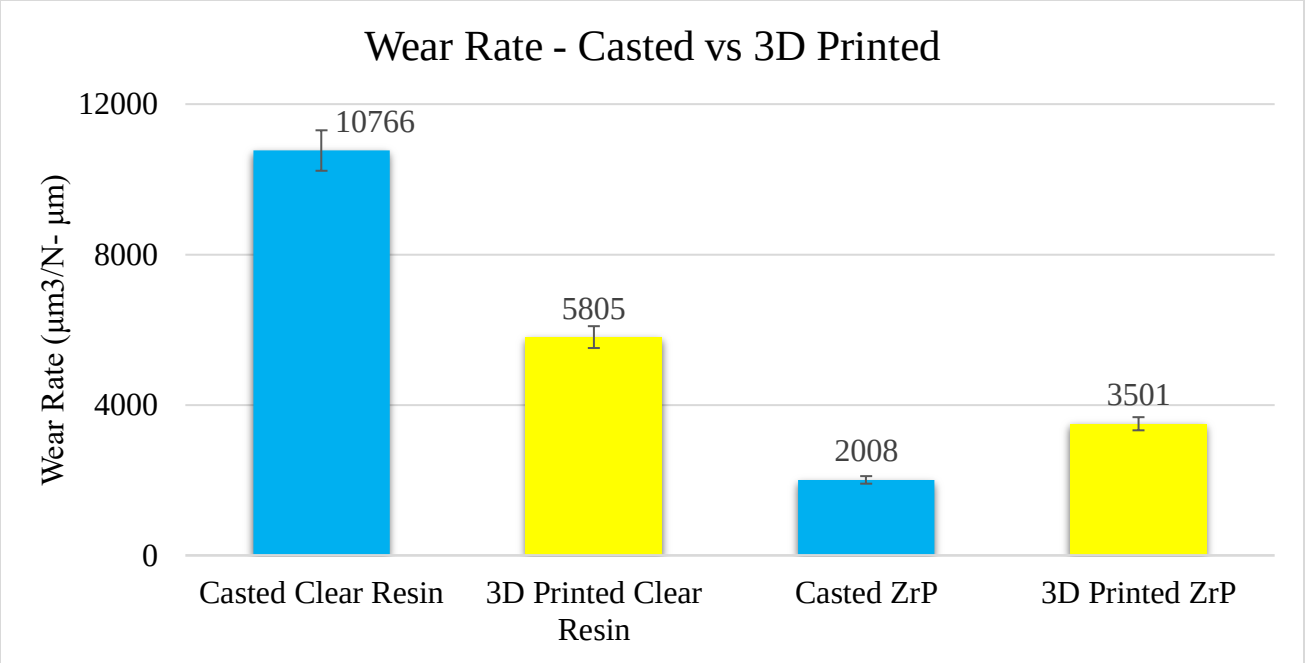

Figure 46. Comparison of wear rate of casted and 3D printed samples

A comparison of the wear rates of the 3D printed and casted specimens indicate that the 3D printed specimens exhibit better wear performance. The 3D printed specimens showed ~40% less wear as compared to the casted specimens. This can be attributed to the layer-by-layer printing process used in SLA. This is discussed in detail in section 5.3.

5.3. Mechanism of α-ZrP NPs on tribological performance of 3D printed parts

The experimental results discussed in section 5.1 and 5.2 indicate that low concentrations of α-ZrP significantly reduced friction and wear of 3D printed nanocomposites. The results also indicated that 3D printing improved the wear resistance of the nanocomposite specimens.

As discussed in Chapter IV, the disc-like shape of the α-ZrP nanoplatelets, along with their layered structure, play a critical role in enhancing the friction and wear performance of the nanocomposites. The disc-like shape of the nanoplatelets allows them to enter into the contact region between the mating surfaces. These nanoplatelets carry a load on their surfaces which in turn reduces the effective load and contact-area of the mating surfaces. By effectively reducing the contact area of asperities on the mating surfaces, the NPs reduce cold welding of asperities and lower the amount of adhesive wear. This also lowers the shear stress, which is effective in reducing the friction between the contact surfaces.

Alongside, the layered structure of α-ZrP nanoplatelets, which has been discussed in detail in Chapter IV (section 4.3), consist of relatively weak hydrogen bonds between the adjacent layers. Under a shearing force, these bonds allow the adjacent layers to be easily exfoliated. This leads to easier and more efficient dispersion of wear energy.

In the present study, in conditions of 3D printing, objects are printed layer-by-layer, with each layer thickness equal to the print resolution. We set the printing resolution to 100 μm. The layer-by-layer printing process led to improved alignment of the α-ZrP NPs with each layer of 3D printed specimen. This is illustrated in figure 5.8. This improved alignment of α-ZrP nanodiscs leading to homogenous distribution. In particular, aligned particles promote effective reduction of friction due more organized weaker van der Walls forces between discs. This is further evidenced when comparting the samples between casted and 3D printed (Fig.46). As a result, the friction of 3D printed samples has lower coefficient of friction than casted. Without agglomeration and favorable

homogenous particle distribution (Fig.47), the interfacial strength between particles and polymer matrix is uniform and strong. All those factors are favorable to reduce wear.

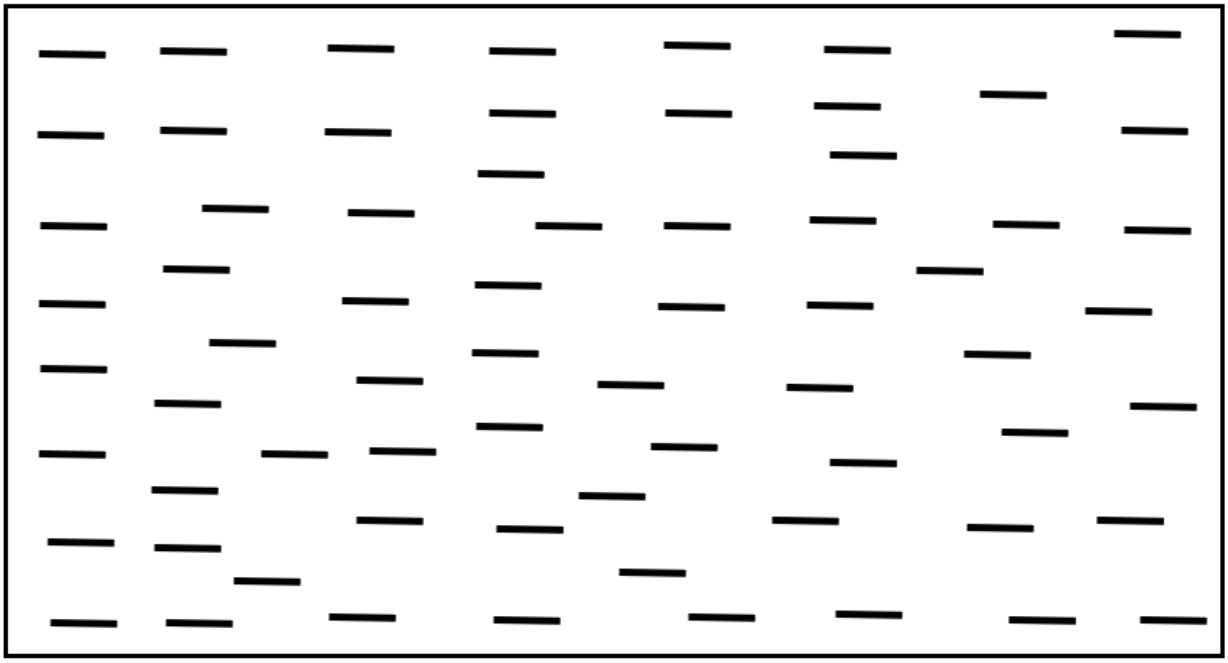

Figure 47. Alignment of α-ZrP discs –3D printed

CHAPTER VI

CONCLUSION & FUTURE RECOMMENDATIONS

In this thesis research we conducted the design, synthesis and tribological evaluation of a novel photopolymer nanocomposite, using α-ZrP nanoparticles as nanofillers. Two approaches were used to fabricate the materials, cast verses 3D printed. The tribological performance of the photopolymer nanocomposites were investigated using a pin-on-disc tribometer at room temperature. The results obtained from the experiments led to the following conclusions and future recommendations.

6.1. Conclusions

Sample materials of photopolymer nanocomposites were fabricated by casting and 3D printing. The matrix was standard clear resin, and α-ZrP nanoparticles were used as additives. Design of experiments used nanoparticle concentration as the independent variable. The concentration of nanoparticles was evaluated from 0% to 1%. Major findings are discussed below:

1. Samples with 0.1 % wt. of α-ZrP nanoparticles showed promising results. At this concentration, friction and wear performances were significantly improved. As the concentration is increased, the performance enhancement diminishes due to the non-uniform dispersion and agglomeration of nanoparticles.
2. Among samples fabricated through 3D printing, specimens with 0.1 % wt. of α-ZrP nanoparticles showed an impressive 65% reduction in wear and a 34% reduction in friction.

Similar to 3D printing, casted specimens with 0.1 % wt. of of α-ZrP nanoparticles showed a notable 67% reduction in wear and a 32% reduction in friction.

3. In comparison between fabrication processes of casting and 3D printing, it was observed that 3D printing significantly improves the wear resistance of specimens. 3D printed specimens exhibited ~40% less wear as compared to the casted specimens.
4. The principles behind the results have been discussed in chapters IV and V. The main reason for the performance improvement is the disc-like shape of the α-ZrP nanoparticles and the weak links between the discs which allow for easy and efficient dispersion of wear energy. This along with the layer-by-layer printing approach (employed in stereolithography), significantly restrains surface deformation and improves wear resistance of specimens.

The findings of this research are beneficial to the advanced manufacturing and polymer nanocomposite industry, and open up new arenas for the use of α-ZrP nanoparticles as anti-friction and anti-wear additives in stereolithographic printing, for fabricating high performance polymer-based photoactivated nanocomposites.

6.2. Future Recommendations

1. Analyze the influence of print resolution on the tribological performance of 3D printed photopolymer nanocomposites:

In this study we have used a print resolution of 100 µm. Parts printed at different resolutions need to be tested to have a better understanding of print resolution on tribological performance of 3D printed nanocomposites.

2. Examine different post-curing processes (natural sunlight, specialized post-curing equipment etc.) and their effects on the tribological performance of 3D printed nanocomposites.

   Post-curing processes (involving light and heat treatment) further enhance performance of 3D printed parts. Different post-curing processes influence the material properties differently, depending on the wavelength of UV light used, energy density of light source etc.

REFERENCES

1. Associates, W., Wohlers Report 2015: 3D Printing and Additive Manufacturing State of the Industry Annual Worldwide Progress Report. 2015.
2. McCue, T. Significant 3D Printing Forecast Surges To $35.6 Billion. 2019; Available from: https://www.forbes.com/sites/tjmccue/2019/03/27/wohlers-report-2019-forecasts-35-6-billion-in-3d-printing-industry-growth-by-2024/#44450c417d8a.
3. Melchels, F.P., J. Feijen, and D.W. Grijpma, A review on stereolithography and its applications in biomedical engineering. Biomaterials, 2010. 31(24): p. 6121-30.
4. Andrzejewska, E., Photopolymerization Kinetics of Multifunctional Monomers. Progress in Polymer Science, 2001. 26: p. 605-665.
5. Formlabs. Guide to Stereolithography (SLA) 3D Printing in 2019. 2019; Available from: https://formlabs.com/blog/ultimate-guide-to-stereolithography-sla-3d-printing/.
6. Fouassier, J.-P. Photoinitiation, photopolymerization, and photocuring : fundamentals and applications. Munich; New York; Cincinnati: Hanser ; Distributed by Hanser/Gardner Publications.
7. Gillham, J.K., Award address formation and properties of network polymeric materials. Polymer Engineering & Science, 1979. 19(10): p. 676-682.
8. Wendel, B., et al., Additive Processing of Polymers. Macromolecular Materials and Engineering, 2008. 293(10): p. 799-809.
9. Maruo, S. and K. Ikuta, Submicron stereolithography for the production of freely movable mechanisms by using single-photon polymerization. Sensors and Actuators A: Physical, 2002. 100(1): p. 70-76.

10. Hutmacher, D.W., M. Sittinger, and M.V. Risbud, Scaffold-based tissue engineering: rationale for computer-aided design and solid free-form fabrication systems. Trends Biotechnol, 2004. 22(7): p. 354-62.
11. Gabbrielli, R., I. Turner, and C. Bowen, Development of Modelling Methods for Materials to be Used as Bone Substitutes. Key Engineering Materials - KEY ENG MAT, 2008. 361-363: p. 903-906.
12. Mankovich, N.J., et al., Surgical planning using three-dimensional imaging and computer modeling. (0030-6665 (Print)).
13. Bártolo, P. and I. Gibson, History of Stereolithographic Processes. 2011. p. 37-56.
14. Latouche, M. SLA 3D Printing materials compared. 2019; Available from: https://www.3dhubs.com/knowledge-base/sla-3d-printing-materials-compared/.
15. Formlabs. Materials Data Sheet. Photopolymer Resin for Form 1+ and Form 2 2019; Available from: https://formlabs-media.formlabs.com/datasheets/Standard-DataSheet.pdf.
16. Carnes, K., et al., The ten greatest events in tribology history. 2005. **61**: p. 38-47.
17. Dowson, D., The History of Tribology in America. Journal of Tribology, 1981. **103**(3): p. 323-333.
18. Jost, H., Tribology: How a word was coined 40 years ago. ARCHIVE Proceedings of the Institution of Mechanical Engineers Part J Journal of Engineering Tribology 1994-1996 (vols 208-210), 2009. **223**: p. 240-244.
19. Pope, J.E., Tribology. Rules of Thumb for Mechanical Engineering. 1996: Gulf Professional Publishing. 406.
20. S.K. Basu, S.N.S., B.B. Ahuja, Introduction to tribology. Fundamentals of Tribology. 2005.

21. Ian Hutchings, P.S., Introduction. Tribology: Friction and Wear of Engineering Materials. 2017: Butterworth-Heinemann.
22. Wills, J.G., Lubrication fundamentals. 1990, United States: Marcel Dekker Inc.
23. Bhushan, B. and P. Ko, Introduction to Tribology. Applied Mechanics Reviews, 2003. **56**: p. B6.
24. Seireg, A.A., Introduction. Friction and Lubrication in Mechanical Design. 1998.
25. Seireg, A.A., Friction and Lubrication in Rolling/Sliding Contacts. Friction and Lubrication in Mechanical Design. 1998.
26. Lubricants in the Tribological System, in Lubricants and Lubrication. p. 7-22.
27. Seireg, A.A., Wear. Friction and Lubrication in Mechanical Design. 1998.
28. Shipway, P.H., Fretting Wear, in Friction, Lubrication, and Wear Technology. 2017, ASM International. p. 0.
29. Zaferani, S., Introduction of polymer-based nanocomposites. 2018. p. 1-25.
30. Cai, N., et al., Preparation and properties of nanodiamond/poly(lactic acid) composite nanofiber scaffolds. Fibers and Polymers, 2014. **15**(12): p. 2544-2552.
31. Liu, L., et al., Effects of hard and soft components on the structure formation, crystallization behavior and mechanical properties of electrospun poly(l-lactic acid) nanofibers. Polymer, 2013. **54**(19): p. 5250-5256.
32. McCullen, S.D., et al., Electrospun composite poly(L-lactic acid)/tricalcium phosphate scaffolds induce proliferation and osteogenic differentiation of human adipose-derived stem cells. Biomed Mater, 2009. **4**(3): p. 035002.
33. Ribeiro Neto, W.A., et al., Influence of the microstructure and mechanical strength of nanofibers of biodegradable polymers with hydroxyapatite in stem cells growth.

Electrospinning, characterization and cell viability. Polymer Degradation and Stability, 2012. 97(10): p. 2037-2051.

34. Kurtycz, P., et al., Electrospun poly(L-lactic)acid/nanoalumina (PLA/Al2O3) composite fiber mats with potential biomedical application — Investigation of cytotoxicity. Fibers and Polymers, 2013. 14(4): p. 578-583.

35. Kurtycz, P., et al., Biodegradable polylactide (PLA) fiber mats containing Al2O3-Ag nanopowder prepared by electrospinning technique — Antibacterial properties. Fibers and Polymers, 2013. 14(8): p. 1248-1253.

36. Ji, X., et al., Effect of nanoscale-ZnO on the mechanical property and biocompatibility of electrospun poly(L-lactide) acid/nanoscale-ZnO mats. J Biomed Nanotechnol, 2013. 9(3): p. 417-23.

37. Kumar, C.S.S.R., Nanotechnology Characterization Tools for Biosensing and Medical Diagnosis. 2018: Springer-Verlag Berlin Heidelberg.

38. He, X., H. Liang, and Texas A & M University, Synthesis, Characterization, Properties, and Tribological Performance of 2D Nanomaterials. 1 online resource.

39. Dai, Y., H. Xu, and J. Dong, Lubrication Performance of α-Zirconium Phosphates as an Anti-Wear Additive in Vegetable Oil-Based Anhydrous Calcium Grease. Lubricants, 2018. 6: p. 63.

40. Bahadur, S. and C. Sunkara, Effect of transfer film structure, composition and bonding on the tribological behavior of polyphenylene sulfide filled with nano particles of TiO2, ZnO, CuO and SiC. Wear, 2005. 258: p. 1411-1421.

41. Wang, Q.-H., et al., The effect of nanometer SiC filler on the tribological behavior of PEEK. Wear, 1997. **209**(1): p. 316-321.

42. Wang, Q., et al., The friction and wear properties of nanometer ZrO2-filled polyetheretherketone. Journal of Applied Polymer Science, 1998. **69**(1): p. 135-141.

43. Schwartz, C.J. and S. Bahadur, Studies on the tribological behavior and transfer film–counterface bond strength for polyphenylene sulfide filled with nanoscale alumina particles. Wear, 2000. **237**(2): p. 261-273.

44. Sawyer, W.G., et al., A study on the friction and wear behavior of PTFE filled with alumina nanoparticles. Wear, 2003. **254**(5): p. 573-580.

45. Karimi, H., Preparation of Zirconium Phosphate Nanoparticles and Its Application in the Protection of Aldehydes. Journal of Sciences, Islamic Republic of Iran, 2017. **28**(4): p. 313-323.

46. Xiao, H., et al., Amine-intercalated α-zirconium phosphates as lubricant additives. Applied Surface Science, 2015. **329**: p. 384-389.

47. Xingliang He, H.X., Hyunho Choi, Agustín Díaz, Brian Mosby, Abraham Clearfield, Hong Liang, α-Zirconium phosphate nanoplatelets as lubricant additives. Colloids and Surfaces A: Physicochemical and Engineering Aspects, 2014. **452**: p. 32-38.

48. Dai, W., et al., Formation of Anti-Wear Tribofilms via α-ZrP Nanoplatelet as Lubricant Additives. Lubricants, 2016. **4**: p. 28.

49. Sun, L., et al., Preparation of α-zirconium phosphate nanoplatelets with wide variations in aspect ratios. New Journal of Chemistry, 2007. **31**(1): p. 39-43.

50. W. Müller-Warmuth, R.S., Progress in Intercalation Research. Physics and Chemistry of Materials with Low-Dimensional Structures. 1994: Springer Netherlands. XIV, 514.

51. Xie, H., et al., Lubrication performance of MoS2 and SiO2 nanoparticles as lubricant additives in magnesium alloy-steel contacts. Tribology International, 2016. **93**: p. 63-70.

52. Hu, K.H., et al., Tribological properties of molybdenum disulfide nanosheets by monolayer restacking process as additive in liquid paraffin. Tribology International, 2009. **42**(1): p. 33-39.

53. Kogovšek, J., et al., Influence of surface roughness and running-in on the lubrication of steel surfaces with oil containing MoS2 nanotubes in all lubrication regimes. Tribology International, 2013. **61**: p. 40-47.

54. Mosleh, M., et al., Modification of sheet metal forming fluids with dispersed nanoparticles for improved lubrication. Wear, 2009. **267**(5): p. 1220-1225.

55. Kalin, M., et al., The Formation of Tribofilms of MoS2 Nanotubes on Steel and DLC-Coated Surfaces. Tribology Letters, 2014. **55**.

56. Kogovšek, J., M. Remškar, and M. Kalin, Lubrication of DLC-coated surfaces with MoS2 nanotubes in all lubrication regimes: Surface roughness and running-in effects. Wear, 2013. **303**(1): p. 361-370.

57. Lahouij, I., et al., IF-MoS2 based lubricants: Influence of size, shape and crystal structure. Wear, 2012. **296**(1): p. 558-567.

58. Formlabs. Clear Photoreactive Resin for Formlabs 3D printers. Formlabs Materials Sheet 2019; Available from: https://archive-media.formlabs.com/upload/Clear__Resin_SDS_EU.pdf.

59. Stickler, M. and T. Rhein, Polymethacrylates. Ullmann's Encyclopedia of Industrial Chemistry, 2000.

60. Formlabs. Materials Data Sheet. Formlabs Resin for Form1+ and Form2 2019; Available from: https://archive-media.formlabs.com/upload/XL-DataSheet.pdf.

61. CalTech, L. What is an Interferometer? LIGO - A Gravitational-Wave Interferometer 2015; Available from: https://www.ligo.caltech.edu/page/what-is-interferometer.

62. Britannica, T.E.o.E., Optical interferometer, in Encyclpedia Britannica, T.E.o.E. Britannica, Editor., Encyclopædia Britannica, inc.

63. Di Gianfrancesco, A., 8 - Technologies for chemical analyses, microstructural and inspection investigations, in Materials for Ultra-Supercritical and Advanced Ultra-Supercritical Power Plants, A. Di Gianfrancesco, Editor. 2017, Woodhead Publishing. p. 197-245.

64. Amos, B., Lessons from the history of light microscopy. Nature Cell Biology, 2000. **2**(8): p. E151-E152.

65. Gosens, I., et al., Impact of agglomeration state of nano- and submicron sized gold particles on pulmonary inflammation. Part Fibre Toxicol, 2010. **7**(1): p. 37.

66. Liu, L., et al., Ionothermal Synthesis of Layered Zirconium Phosphates and Their Tribological Properties in Mineral Oil. Inorganic Chemistry, 2010. **49**(18): p. 8270-8275.

67. Joly-Pottuz, L., et al., Ultralow-friction and wear properties of IF-WS2 under boundary lubrication. Tribology Letters - TRIBOL LETT, 2005. **18**: p. 477-485.

68. Greenberg, R., et al., *The Effect of WS2 Nanoparticles on Friction Reduction in Various Lubrication Regimes.* Tribology Letters, 2004. **17**: p. 179-186.